UNIVERSITÉ DE MONTRÉAL

DEVELOPMENT OF THE MICRO-DEPLETION METHOD IN THE CHAIN OF CODES DRAGON4/DONJON4

MAXIME GUYOT
DÉPARTEMENT DE GÉNIE PHYSIQUE
ÉCOLE POLYTECHNIQUE DE MONTRÉAL

MÉMOIRE PRÉSENTÉ EN VUE DE L'OBTENTION DU DIPLÔME DE
MAÎTRISE ÈS SCIENCES APPLIQUÉES
(GÉNIE ÉNERGÉTIQUE)
MARS 2011

UNIVERSITÉ DE MONTRÉAL

ÉCOLE POLYTECHNIQUE DE MONTRÉAL

Ce mémoire intitulé :

DEVELOPMENT OF THE MICRO-DEPLETION METHOD IN THE CHAIN OF CODES DRAGON4/DONJON4

présenté par : GUYOT Maxime,
en vue de l'obtention du diplôme de : Maîtrise ès sciences appliquées
a été dûment accepté par le jury d'examen constitué de :

M. MARLEAU Guy , Ph.D, président.
M. HÉBERT Alain, D.Ing, membre et directeur de recherche.
M. KOCLAS Jean, Ph.D, membre et codirecteur de recherche.
M. DAHMANI Mohamed, Ph.D, membre.

To my family, and my friends...

ACKNOWLEDGMENTS

First, I want to thank my research director, Alain Hébert, for accepting me in this programm, and providing me help during my work in this project.

Then, I would like to thank Elizabeth Varin for her help and advice during my stay in AECL, and after. Her good interventions helped me a lot during my internship to move forward on the project. I thank Mohamed Dahmani for giving me the opportunity to work on this project. Also, I want to thank the AECL employees, working in Montréal, for providing a good atmosphere within the company during my internship.

I also would like to thank the entirety of the member of the *Institut de Génie Nucléaire* from the *École Polytechnique de Montréal* : the teachers for their help when I need it, and the students for the good atmosphere and the support during my master.

Also, I would like to thank all my friends, and the people who supported me in Montréeal, or elsewhere, for making this stay in Montréal such a great experience.

RÉSUMÉ

Ce projet a pour but de développer et de tester la méthode de micro-évolution dans le code DONJON. Classiquement, on utilise 2 niveaux de calculs pour réaliser une simulation numérique de coeur. Le code de cellule (DRAGON) est utilisé pour générer des bases de données réacteurs. Il évalue les sections efficaces condensées et homogénéisées pour différents paramètres locaux ou globaux. Ces bases de données sont ensuite interpolées par le code de coeur pour calculer les taux de réactions et les puissances de grappes sur tout le coeur. L'évolution du coeur est alors réalisée de manière "macroscopique".

Une méthode alternative est de faire l'évolution du combustible dans le code de coeur, en résolvant numériquement les équations d'évolution pour chaque grappe. Cette technique possède l'avantage d'utiliser les grandeurs locales pour calculer les nouvelles concentrations isotopiques. On peut avoir ainsi une meilleure prise en compte de certains produits de fission. Une méthode basée sur l'interpolation ne tient pas compte directement du flux local, mais plutôt de l'usure du combustible. Pour diminuer les erreurs dues à l'interpolation, on utilise un module correctif. Le but de ce module est de corriger la distribution de Xénon 135 dans le coeur, en fonction du niveau de puissance local. Le Xénon-135 est un isotope important lors du fonctionnement d'un réacteur à cause de sa forte section efficace d'absorption. Il est important qu'il soit corrigé pour diminuer les erreurs sur la réactivité.

Une démarche progressive est utilisée dans ce document pour étudier les principaux phénomènes liés à cette méthode. On étudie d'abord 2 benchmarks simples avec différentes conditions, en comparaison avec un calcul de transport DRAGON. Le calcul DRAGON sert ici de référence. Il est réalisé sur une géometrie détaillée comprenant les 37 crayons de combustible de la grappe, avec les gaines en zirconium. Les calculs DONJON sont faits en diffusion sur des mélanges homogènes. On teste notamment le gain apporté par la micro-évolution vis-à-vis d'un calcul d'interpolation pour différents niveaux de puissance. Ces benchmarks sont réalisés sur des assemblages de cellules CANDU. La principale conclusion de ces études est l'amélioration notable du calcul du facteur de multiplication des assemblages évoluants à faible puissance, lorsqu'on utilise la micro-évolution.

Finalement, on utilise les deux méthodes d'évolution programmées dans DONJON sur un suivi de coeur CANDU pendant une cinquantaine de jours. Environ 30 schémas de calculs sont exécutés les uns après les autres selon différentes méthodes. Tout d'abord, on réalise

le calcul “classique” avec une interpolation de la base de données. On ajoute à ce schéma de calcul un module de correction de la distribution de Xénon. 2 calculs d'évolution sont effectués pour le suivi de coeur avec 2 homogénéisations différentes pour tenir compte des hétérogénéités des cellules CANDU. On peut ainsi faire évoluer séparement les rangées de crayons constituants chaque grappe.

Les conclusions de l'étude du suivi de coeur sont les suivantes. En terme de facteur de multiplication, le choix d'une méthode ou d'une autre n'apporte pas un changement important. Les effets d'un calcul de type micro-évolution sont supposés être locaux et donc n'ont que peu d'impact sur le calcul d'une grandeur globale comme le k_{eff} d'un réacteur complet. On observe cependant une meilleure évaluation des puissances en périphérie du réacteur avec la micro-évolution. On remarque aussi que les concentrations de Xénon-135 sont largement faussées par le calcul interpolatif sur les grappes situées au extrémité du coeur. La correction de la distribution de Xénon permet de diminuer ces écarts.

ABSTRACT

This project is dedicated to the development of the micro-depletion method in the chain of codes DRAGON/DONJON. A full-core calculation is usually a two-level computational scheme. Two different computational codes are required to perform such a calculation: a lattice code (DRAGON in our case) and a diffusion code (DONJON in our case). A lattice calculation is done to generate multi-parameter reactor databases. Theses tables are compatible with the diffusion code. We can use them to compute the fluxes over the reactor using a diffusion approximation. In this case, the fuel depletion in the core is realized by the computation of new burnups, thanks to the local power levels.

The micro-depletion method is based on the numerical solution of the depletion equations, also called as the Bateman equations. In each bundle, isotopic concentrations are available to compute the reaction rates, and perform the depletion. At each burnup step, these concentrations are updated with the aid of a depletion equations solver. The main advantage of this method, in comparison to an interpolation computation, is the consideration of local effects. While solving the depletion equations, local reaction rates are used to find the new densities. When we interpolate the databases, only the burnup of the fuel is used to get new nuclear properties. However, some fission products are more dependent on the actual flux they are exposed to than on the energy released during the operation time of the core. This is the case for Xenon-135. Because of the huge absorption cross section of Xenon-135, this isotope plays an important role in the reactor behaviour. To investigate this problem, a module is written to compute the Xenon distribution in the DONJON code. This module is used in an interpolation calculation to correct the densities estimated by the database.

A step-by-step approach is used in this document. The goal is to underline the main contribution by using micro-depletion method. Two Benchmarks are studied using a reference DRAGON calculation. Different power levels are tested to put emphasis on the consideration of local effects according to the two methods. We observe that the effective multiplication factor tends to be biased for low power macroscopic depletion calculations. Certain interpolated isotopic concentrations are biased because they correspond to nominal power concentrations.

INTRODUCTION

Since nuclear power is used to produce electricity, computational codes have been developed to simulate the behaviour of these reactors. As new reactors and new fuels are studied and invented, the development of new computational techniques is at a crucial point. Because of the complexity of a reactor, a two-level computational scheme is generally used to simulate a full core. Therefore, two types of deterministic codes are required. The first is a lattice code, used to generate nuclear properties of the different materials in the reactor. The nuclear cross sections are stored in databases readable by the second code. The second level is composed of a diffusion code used to compute the neutron flux over the whole reactor.

Until the end of this document, the two codes used are DRAGON and DONJON Version4 respectively [1]. They have been both developed at Ecole Polytechnique de Montréal.

The goal of our study is to develop and to test the micro-depletion capability of DONJON. Until now, the classic method used to follow a core is based on an interpolation process. A multi-parameter database previously generated by DRAGON is used to compute the nuclear properties at each time step. A computation of power distribution is required to perform the depletion, and to compute the new burnups. An alternative method, the micro-depletion method, is based on solving the depletion equations. Such a method is already implemented and successfully tested by other computational codes [2] [3].

The global mechanism of microscopic depletion is to compute isotopic densities at core level. The new concentrations N are used to compute macroscopic cross sections $\Sigma = N\sigma$. In a macroscopic depletion calculation scheme, burnup steps are carried out without the need of microscopic quantities such as microscopic cross sections or isotopic densities. The macroscopic cross sections are used for flux, power and burnup calculations in this case. The microscopic depletion calculation scheme is expected to improve the treatment of local effects. Let us consider, for instance, two fuel bundles, one in the core center, and one at its border. Suppose that these bundles have the same average power. As a consequence, their burnup evolution will be the same. However, the flux of the bundle located at the core center is less thermal than the bundle at the core border. So the microscopic depletion of these two bundles will be different.

This document presents the development and the validation of this new method. The final point is to implement the micro-depletion calculation scheme of a CANDU-6 reactor. A comparison can therefore be done with a classic core-follow.

The first chapter explains the theoretical background required to understand the study. Reactor physic concepts are introduced.

The second chapter provides elements of comparison between the classic macro-depletion calculation scheme and the micro-depletion calculation scheme. The main features of each method are presented.

The third chapter gives elements of validation and comparison of the micro-depletion method. Two types of test cases are studied, and compared with a DRAGON4 reference. Multiplication factors and isotopic densities were examinated under different conditions. This study will allow us to get some preliminary conclusions, before testing the method on a full core of CANDU-6. Particularly, the treatment of fission products differs from one method to another.

Finally, the fourth chapter contains a complete study of the CANDU-6 core follow-up. The two depletion methods are tested and a discussion of the methods is provided in this chapter as well.

The final chapter is dedicated to the study of a CANDU-6 follow-up. Several calculations are performed one after the other using different methods. The `XENON:` module is used to correct the Xenon distribution in the whole core. For the micro-depletion, the possibility to deplete separately the fuel pins is realized.

In terms of effective multiplication factor, the micro-depletion turns out to be very close to the interpolation calculation. It is not surprising as the improvements due to the micro-depletion method are supposed to be local rather than global. The core multiplication factor is not an indicator of the accuracy of the results in this case. However, the study of the axial power distribution comparison shows a difference in the peripheral planes of the CANDU-6 reactor. For instance, the powers of peripheral bundles are underestimated with the macro-depletion method and the powers at the middle of the core are overestimated. The Xenon distribution correction improves the evaluation of Xenon concentrations. The impact of this correction on power distribution is however minor.

CONTENTS

LIST OF TABLES

LIST OF FIGURES

LIST OF APPENDICES

LIST OF ACRONYMS AND ABBREVIATIONS

CANDU	Canada Deuterium Uranium
API	Application Programing Interface
k_{eff}	Effective multiplication factor
mk	Unit of reactivity : One Milli-k is a reactivity of 0.001
JEFF	Joint Evaluated Fission and Fusion
FPD	Full Power Day
MCFD	Mesh Centered Finite Difference
PWR	Pressurized Water Reactor

CHAPTER 1

GENERAL CONCEPTS OF REACTOR PHYSICS

This chapter aims at giving a theoretical knowledge to understand the work done in this project. The first step is to introduce the particle flux, which is the solution of the transport equation. Except in few theoretical cases, the transport equation cannot be solved without the use of numerical methods. These methods are briefly introduced in this Chapter. The numerical solution of the transport equation is also facilitated by performing a multigroup discretization in energy. The formalism used is the same as presented by A. Hébert in the book Applied Reactor Physics [4]. General information can also be found in References [5] [6].

1.1 Theoretical concepts

1.1.1 The particle flux

In a nuclear reactor such as CANDU-6, the power production is made by fission reactions. A fission reaction is initiated by bombarding neutron on a fissile nucleus, such as Uranium-235. The initial heavy nucleus splits generally in two fragments. A certain amount of prompt neutrons are also released. The maximum recoverable energy by fission is about 200 MeV. An example of such a reaction is given below:

$$^{235}U + n \rightarrow {}^{236}U^{*} \rightarrow {}^{135}Xe + {}^{98}Sr + 3n \tag{1.1}$$

The neutrons generated by fission are very energetic. In a thermal reactor, these neutrons should be slowed down before being able to initiate a new reaction. Fission reactors are based on a self-sustaining chain reaction. The transport theory is introduced to describe the population of neutrons. During the operation of a reactor, it is very important to monitor and to be able to determine the neutron population at each time. In a reactor, each particle is identified by a set of seven variables. These quantities are :

- three position co-ordinates : $\mathbf{r} = x\mathbf{i} + y\mathbf{j} + z\mathbf{k}$
- three velocity co-ordinates : the velocity module $V_n = |V_n|$ and the two components of the direction $\mathbf{\Omega} = \frac{V_n}{|V_n|}$
- the time t

The neutron population is described by its density $n(\mathbf{r}, V_n, \mathbf{\Omega}, t)$ so that $n(\mathbf{r}, V_n, \mathbf{\Omega}, t) d^3r d^2\Omega$ dV_n is the number of particles at time t, in the volume element d^3r surrounding $\mathbf{r}$, in the velocity element dV_n surrounding V_n and in the solid angle $d^2\Omega$ surrounding $\mathbf{\Omega}$. From this definition, we introduce the angular flux as :

$$\phi(\mathbf{r}, V_n, \mathbf{\Omega}, t) = V_n \times n(\mathbf{r}, V_n, \mathbf{\Omega}, t) \tag{1.2}$$

In many applications, knowing or determining the angular dependence is not important so we reduce the flux distribution by integrating equation 1.2 over variable $\mathbf{\Omega}$. Therefore, we introduce the integrated flux as :

$$\phi(\mathbf{r}, V_n, t) = \int_{4\pi} d^2\Omega \phi(\mathbf{r}, V_n, \mathbf{\Omega}, t) \tag{1.3}$$

Another fundamental quantity is the angular current. This current is a distribution defined by equation 1.4.

$$\mathbf{J}(\mathbf{r}, V_n, \mathbf{\Omega}, t) = \mathbf{\Omega} \phi(\mathbf{r}, V_n, \mathbf{\Omega}, t) \tag{1.4}$$

In the same way as for the flux, we introduce the integrated current, to dispose of the angular dependence, in equation 1.5.

$$\mathbf{J}(\mathbf{r}, V_n, t) = \int_{4\pi} d^2\Omega \mathbf{J}(\mathbf{r}, V_n, \mathbf{\Omega}, t) \tag{1.5}$$

1.1.2 The concept of cross sections

The neutron-nucleus collision can result in a variety of nuclear reactions. Each type of nuclear reaction x is characterized by a microscopic cross section $\sigma_{x,i}$. This quantity represents the probability of occurence of the reaction x on a nucleus i. A cross section is dependent on the energy of the neutron and on the target nuclide. It has the dimension of a surface and is expressed in barn ($1barn = 10^{-24} cm^2$). We can also define the macroscopic cross section of a reaction x for an isotope i with a number density of N_i nuclei per unit volume :

$$\Sigma_{x,i}(E) = \sigma_{x,i}(E) N_i \tag{1.6}$$

For a material composed of different isotopes, the resulting macroscopic cross section is :

$$\Sigma_x(E) = \sum_i \Sigma_{x,i}(E) \tag{1.7}$$

The total macroscopic cross section of a region takes into account all the nuclear reactions.

$$\Sigma(E) = \sum_x \Sigma_x(E) \tag{1.8}$$

1.1.3 Presentation of the transport equation

The transport equation is a balance relation of the neutron population in an hyper volume $dV_n d^3r d^2\Omega$, surrounding $\{V_n, \mathbf{r}, \mathbf{\Omega}\}$. The time-dependent transport equation is written in Equation 1.9:

$$\frac{1}{V_n}\frac{\partial}{dt}\phi(\mathbf{r}, V_n, \mathbf{\Omega}, t) + \mathbf{\Omega}.\nabla\phi(\mathbf{r}, V_n, \mathbf{\Omega}, t) + \Sigma(\mathbf{r}, V_n, t)\phi(\mathbf{r}, V_n, \mathbf{\Omega}, t) = Q(\mathbf{r}, V_n, \mathbf{\Omega}, t) \tag{1.9}$$

where

- $\frac{1}{V_n}\frac{\partial}{dt}\phi(\mathbf{r}, V_n, \mathbf{\Omega}, t)$ represents the time-rate of change in the neutron density. This term is absent in steady-state conditions.
- $\mathbf{\Omega}.\nabla\phi(\mathbf{r}, V_n, \mathbf{\Omega}, t)$ represents the neutron streaming. This is also called the transport term.
- $\Sigma(\mathbf{r}, V_n, t)\phi(\mathbf{r}, V_n, \mathbf{\Omega}, t)$ represents all the interactions that cause the loss of neutrons.
- $Q(\mathbf{r}, V_n, \mathbf{\Omega}, t)$ represents the source term. This term is composed of fission, scattering and delayed neutron production terms.

In steady-state conditions, the first term on the left-hand side of the transport equation can be removed to obtain the following equation:

$$\mathbf{\Omega}.\nabla\phi(\mathbf{r}, V_n, \mathbf{\Omega}) + \Sigma(\mathbf{r}, V_n)\phi(\mathbf{r}, V_n, \mathbf{\Omega}) = Q(\mathbf{r}, V_n, \mathbf{\Omega}) \tag{1.10}$$

In the following developments, the neutron energy $E = \frac{1}{2}m{V_n}^2$ is used instead of the neutron velocity V_n:

$$\mathbf{\Omega}.\nabla\phi(\mathbf{r}, E, \mathbf{\Omega}) + \Sigma(\mathbf{r}, E)\phi(\mathbf{r}, E, \mathbf{\Omega}) = Q(\mathbf{r}, E, \mathbf{\Omega}) \tag{1.11}$$

1.1.4 Source density

The sources term Q is composed of a fission and a scattering term. The scattering term is composed of elastic or inelastic diffusions, and (n,xn) reactions. To write the term of source, we consider that the scattering cross section Σ_s takes into account the different phenomena. Generally, this cross section is not isotropic and depends on the energy and the direction of the initial neutron.

$$Q^{scat}(\mathbf{r}, E, \mathbf{\Omega}) = \int_{4\pi} d^2\Omega' \int_0^{+\infty} dE' \Sigma_s(\mathbf{r}, E \leftarrow E', \mathbf{\Omega} \leftarrow \mathbf{\Omega}')\phi(\mathbf{r}, E', \mathbf{\Omega}') \tag{1.12}$$

where

– $\Sigma_s(\mathbf{r}, E \leftarrow E', \mathbf{\Omega} \leftarrow \mathbf{\Omega}')$ is the macroscopic differential scattering cross section from energy E to energy E' and from solid angle $\mathbf{\Omega}$ to solid angle $\mathbf{\Omega}'$

We consider the materials isotropic, so the scattering cross section depends only on the scattering angle $\mathbf{\Omega}.\mathbf{\Omega}'$. Equation 1.12 can be then written :

$$Q^{scat}(\mathbf{r}, E, \mathbf{\Omega}) = \int_{4\pi} d^2\Omega' \int_0^{+\infty} dE' \Sigma_s(\mathbf{r}, E \leftarrow E', \mathbf{\Omega}.\mathbf{\Omega}')\phi(\mathbf{r}, E', \mathbf{\Omega}') \tag{1.13}$$

It is convenient to expand the scattering cross section in terms of Legendre polynomials P_l :

$$\Sigma_s(\mathbf{r}, E \leftarrow E', \mathbf{\Omega}.\mathbf{\Omega}') = \sum_{l=1}^{L} \frac{2l+1}{2} \Sigma_{s,l}(\mathbf{r}, E \leftarrow E') P_l(\mathbf{\Omega}.\mathbf{\Omega}') \tag{1.14}$$

where

– L is the maximum scattering order after which the sum is truncated.

– $\Sigma_{s,l}(\mathbf{r}, E \leftarrow E')$ are the Legendre coefficients of the scattering cross section.

Since the fission neutrons are emitted isotropically, the corresponding source term is independent of $\mathbf{\Omega}$.

$$Q^{fiss}(\mathbf{r}, E) = \frac{1}{4\pi k_{eff}} \sum_{j=1}^{J} \chi_j(E) \int_0^{+\infty} dE' \nu \Sigma_{f,j}(\mathbf{r}, E')\phi(\mathbf{r}, E') \tag{1.15}$$

where

– $\chi_j(E)$ represents the fission spectrum. This is the probability density that the fission of the j-th isotope produces a neutron of energy E within a dE interval.

– $\Sigma_{f,j}(\mathbf{r}, E')\phi(\mathbf{r}, E')$ is the fission cross section.

– ν is the average number of emitted neutrons per fission.

– J is the number of fissile isotopes.

– k_{eff} is the factor used to divide the fission source in order to maintain steady-state conditions.

Obviously, we have the following relation :

$$Q(\mathbf{r}, E, \mathbf{\Omega}) = Q^{scat}(\mathbf{r}, E, \mathbf{\Omega}) + Q^{fiss}(\mathbf{r}, E) \tag{1.16}$$

1.1.5 Multigroup approach

The resolution of the transport equation is facilitated by performing a multigroup discretization in energy. The multigroup approach consists in dividing the energy continuum to produce a set of G groups. That means that neutrons are assumed to behave as one-speed particles in each group. All the energy dependent quantities are condensed over these groups. The lethargy variable $u = ln(\frac{E_0}{E})$ can also be used :

$$W_g = \{u, u_{g-1} \leq u < u_g\} = \{E, E_g < E \leq E_{g-1}\}, \forall g \in \{1, .., G\} \tag{1.17}$$

E_0 is set to the maximum energy of neutrons in a reactor, and corresponds to $u_0 = 0$. Each group corresponds to an interval $]u_{g-1}, u_g[$ or $]E_g, E_{g-1}[$. We can now rewrite the transport equation in the multigroup form:

$$\mathbf{\Omega}.\nabla\phi_g(\mathbf{r}, \mathbf{\Omega}) + \Sigma_g(\mathbf{r})\phi_g(\mathbf{r}, \mathbf{\Omega}) = Q_g(\mathbf{r}, \mathbf{\Omega}) \tag{1.18}$$

where $g \in \{1, .., G\}$

The group-average values of the flux, the current and the source are defined as :

$$\phi_g(\mathbf{r}, \mathbf{\Omega}) = \int_{u_{g-1}}^{u_g} \phi(\mathbf{r}, u, \mathbf{\Omega}) du \tag{1.19}$$

$$\mathbf{J}_g(\mathbf{r}, \mathbf{\Omega}) = \int_{u_{g-1}}^{u_g} \mathbf{J}(\mathbf{r}, u, \mathbf{\Omega}) du \tag{1.20}$$

$$Q_g(\mathbf{r}, \mathbf{\Omega}) = \int_{u_{g-1}}^{u_g} Q(\mathbf{r}, u, \mathbf{\Omega}) du \tag{1.21}$$

The group-average values of the cross sections are defined in such a way as to preserve the reaction rates.

$$\Sigma_{i,g}(\mathbf{r}, \mathbf{\Omega}) = \frac{1}{\phi_g(\mathbf{r}, \mathbf{\Omega})} \int_{u_{g-1}}^{u_g} \Sigma_i(\mathbf{r}, u, \mathbf{\Omega})\phi(\mathbf{r}, u, \mathbf{\Omega}) du \tag{1.22}$$

$$\Sigma_{s,g\leftarrow h}(\mathbf{r}, \mathbf{\Omega}.\mathbf{\Omega}') = \frac{1}{\phi_h(\mathbf{r}, \mathbf{\Omega})} \int_{u_{g-1}}^{u_g} du \int_{u_{h-1}}^{u_h} du' \Sigma_s(\mathbf{r}, u \leftarrow u', \mathbf{\Omega}.\mathbf{\Omega}')\phi(\mathbf{r}, u, \mathbf{\Omega}) \tag{1.23}$$

where u_{g-1} and u_g are the limits of the energy group g, and u_{h-1} and u_h are the limits of the energy group h.

1.1.6 Boundary conditions

To solve the transport equation, we need to define the boundary conditions. The principle is to close the system of equations. Depending on the computation, different types of boundary conditions can be imposed. Considering a domain V that is surrounded by a boundary ∂V where boundary conditions are applied. Solution of transport equation requires the knowledge of the incoming flux.

Only one type of boundary condition will be used in this document. This condition is the albedo boundary condition, which provides a relation between the incoming flux at the boundary and the outgoing flux. The formula 1.24 makes the relation explicit.

$$\phi(\mathbf{r_s}, \mathbf{V_n}, \mathbf{\Omega}) = \beta\phi(\mathbf{r_s}, \mathbf{V_n}, \mathbf{\Omega}^{'}), \forall \mathbf{r_s} \in \partial V \tag{1.24}$$

where

- $\mathbf{r_s}$ is a point of the boundary ∂V
- $\mathbf{\Omega}^{'}$ is the direction of the outgoing particle.
- $\mathbf{\Omega}$ is the direction of the incoming particle, and therefore, if $\mathbf{N}(r_s)$ is the normal vector, $\mathbf{\Omega}$ verifies $\mathbf{\Omega}.\mathbf{N}(r_s) < 0$.

A boundary condition with $\beta = 0$ is called a vacuum boundary condition while $\beta = 1$ is a reflective boundary condition. For example, a reflective boundary condition can be used to simulate the behavior of a cell surrounded by an infinite lattice of the same cells.

1.1.7 Methods of resolution

Even with the multigroup discretization, the transport equation cannot be solved analytically. Numerical methods must be employed to treat the angular variable. Two different classes of methods are used : stochastic and deterministic methods. Basically, four different deterministic methods are prominently used:

- The methods of characteristics
- The collision probability method
- The discrete ordinates method
- The method of spherical harmonics

In this document, a brief presentation of the diffusion approximation is provided. This corresponds to the method of spherical harmonics, where the angular development of the flux is limited to order 1. This is one of the most common method used in full-core calculations.

Stochastic methods consist in a direct simulation of a neutron population, using a sequence of random numbers to simulate the random events of each particle history.

1.1.8 Homogenization process

The complexity of a real CANDU reactor prevents us from solving the transport equation on a full core. 4560 fuel bundles are present, each one composed of 37 fuel elements. Solving the transport equation on this geometry would be too demanding in computing time. The idea of the homogenization step is to produce homogeneous quantities from the initial heterogeneous system. Only the average values are preserved during this process. Hence, there is a loss of precision.

To perform this step, a reference problem is solved. This problem should be representative of the state of a bundle in the reactor. Generally, we use a CANDU-6 fuel bundle surrounded by some moderator with reflective boundary conditions (see Figure 1.1). It aims to simulate the behavior of a bundle within an infinite lattice obtained by replication of the cell.

To reduce the computational time, a full-core study is done with very few groups of energy. Typically, we use between 2 and 20 energy groups. As the lattice computations are generally done with a few hundred groups, a reduction of the number of groups has to be performed. This condensation process occurs along with the homogenization step.

In this document, the purpose of the homogenization step is to generate useful properties for the diffusion solver TRIVAC, to simulate the CANDU-6 reactor. From this perspective, the homogenization of a detailed CANDU-6 cell will give birth to a 2-group mixture. The Figure 1.1 represents the fuel cell before and after spatial homogenization and energy condensation.

The homogenization/condensation step is performed with the lattice code (DRAGON). The first goal of the homogenization process is to preserve the reaction rates. This step produces a set of cross-sections, constant over a set of energy groups and regions. Homogenized cross-sections are computed using a direct flux-volume weighting. For flux-averaged cross sections, the transport flux is used [7]. If we consider a region V_{merg}, a group g, an

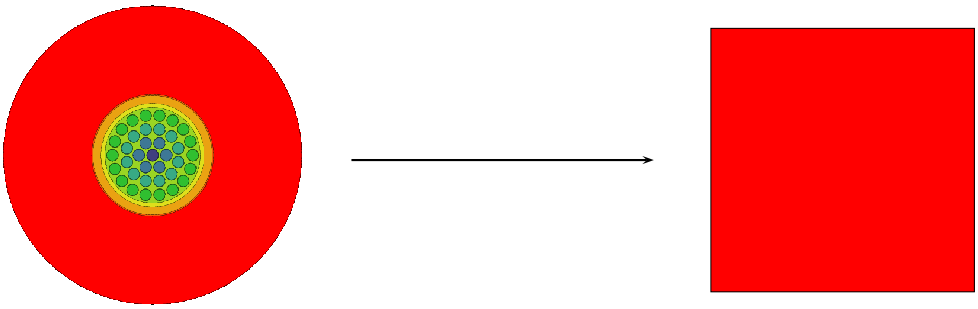

Figure 1.1 Candu-6 cell before and after edition

isotope i and a reaction x, the microscopic and macroscopic cross-sections produced after homogenization are:

$$\overline{\sigma}_{x,i,g} = \frac{1}{\overline{N}_i} \frac{\int_{V_i} dV \int_{E_g} dE\, N_i(r)\, \sigma_{x,i}(r,E)\, \phi(r,E)}{\int_{V_{\text{merg}}} dV \int_{E_g} dE\, \phi(r,E)} \tag{1.25}$$

$$\overline{\Sigma}_{x,i,g} = \overline{N}_i\, \overline{\sigma}_{x,i,g} = \frac{\int_{V_i} dV \int_{E_g} dE\, N_i(r)\, \sigma_{x,i}(r,E)\, \phi(r,E)}{\int_{V_{\text{merg}}} dV \int_{E_g} dE\, \phi(r,E)} \tag{1.26}$$

where

- V_i is a subset of V_{merg}, where the isotope i is defined.
- $\overline{N}_i = \frac{1}{\overline{V}} \int_{V_i} dV N_i(r)$ is the homogenized density for isotope i.
- $\overline{V} = \int_{V_{\text{merg}}} dV$ is the merged volume.

We can point out that the denominator of the previous equation shows the transport flux integrated over the region V_{merg}. This region can differ from the region V_i, where the isotope i is located. This means that isotopes located in different rings of fuel V_i can be homogenized separately, to produce different sets of cross sections.

When an homogenization step is performed, we expect an inevitable loss of certain information. However, an explicit representation of all the heterogeneities of a CANDU-6 fuel cell in the full-core calculation step is not feasible. Different methods have been investigated to reduce this loss of precision. These methods are based on re-introducing local properties of single heterogeneous assemblies in the full-core step [8]. They are commonly named Form Functions Methods. The next subsection gives a brief description of the theory of such methods. It also compares these methods with the capabilities implemented in the chain of codes DRAGON/DONJON.

1.1.9 Form Function Methods

The principle of the Form Function Methods is to incorporate an heterogeneous function in the diffusion flux distribution. This function is generated during the lattice level of the calculation. This factorization can be written :

$$\phi_{reactor} = \phi_{diffusion} \times \psi_{lattice} \tag{1.27}$$

where

- $\phi_{reactor}$ is the reconstructed heterogeneous flux.
- $\phi_{diffusion}$ is the homogeneous flux calculated at core level.
- $\psi_{lattice}$ is the form function evaluated at lattice level. This form function must account for assembly heterogeneities. In a CANDU-6 fuel bundle, the value of the flux is different from one row of pins to an other. Also, the presence of liquid zone controllers can create a variation of the flux.

These form factors should thus be computed and tabulated as function of burnup as other nuclear properties. It should be carried out at the same time as the condensation of the microscopic cross sections.

The use of this reconstruction allows to obtain a more accurate flux distribution. In DRAGON, an alternative method is implemented to make up for the loss of precision at core level due to the homogenization step. Equations 1.25 and 1.26 shows that no additional form factors are required to correct the distribution flux. A pin-by-pin homogenization can be performed to compensate for the loss of precision. At full-core level, the diffusion flux is used to multiply cross sections and produces pin-by-pin reaction rates.

This property of the DRAGON homogenization step can be use to take into account heterogeneities of the CANDU-6 bundle in the full-core calculation step. This particular feature of homogenized cross sections will be used in the fourth Chapter.

1.1.10 Diffusion equation

In a diffusion code, each cell in the reactor contains a single mixture, produced by the edition step of the lattice calculation. One of the major approximations in the diffusion theory is to assume that the flux is only weakly dependent on the angular variables. The linearization of the angular flux can be expressed by equation 1.28:

$$\phi_g(\mathbf{r}, \mathbf{\Omega}) \simeq A_g(\mathbf{r}) + \mathbf{\Omega}.\mathbf{B}_g(\mathbf{r}) \tag{1.28}$$

In the previous development, the two unknowns functions $A_g(\mathbf{r})$ and $\mathbf{B}_g(\mathbf{r})$ can be written in term of known quantities. If we get back to the definition of the integrated flux (1.3), and the integrated neutron current (1.5), we can obtain the expression of the integrated flux given in Equation 1.29.

$$\begin{aligned}
\phi_g(\mathbf{r}) &= \int_{4\pi} d^2\Omega \phi_g(\mathbf{r}, \mathbf{\Omega}) = \int_{4\pi} d^2\Omega [A_g(\mathbf{r}) + \mathbf{\Omega}.\mathbf{B}_g(\mathbf{r})] \\
&= \int_{4\pi} d^2\Omega A_g(\mathbf{r}) + \int_{4\pi} d^2\Omega \mathbf{\Omega}.\mathbf{B}_g(\mathbf{r}) \\
&= A_g(\mathbf{r}) \int_{4\pi} d^2\Omega + \mathbf{B}_g(\mathbf{r}). \int_{4\pi} d^2\Omega \mathbf{\Omega} \\
&= 4\pi A_g(\mathbf{r})
\end{aligned} \tag{1.29}$$

The integrated current provides the second coefficient.

$$\begin{aligned}
\mathbf{J}_g(\mathbf{r}) &= \int_{4\pi} d^2\Omega \mathbf{J}_g(\mathbf{r}, \mathbf{\Omega}) = \int_{4\pi} d^2\Omega \mathbf{\Omega} \phi_g(\mathbf{r}, \mathbf{\Omega}) \\
&= \int_{4\pi} d^2\Omega \mathbf{\Omega} A_g(\mathbf{r}) + \int_{4\pi} d^2\Omega \mathbf{\Omega}\mathbf{\Omega}.\mathbf{B}_g(\mathbf{r}) \\
&= A_g(\mathbf{r}) \int_{4\pi} d^2\Omega \mathbf{\Omega} + \int_{4\pi} d^2\Omega \mathbf{\Omega}\mathbf{\Omega}.\mathbf{B}_g(\mathbf{r}) \\
&= \int_{4\pi} d^2\Omega \mathbf{\Omega}\mathbf{\Omega}.\mathbf{B}_g(\mathbf{r})
\end{aligned} \tag{1.30}$$

To obtain the relations, we have used the two following identities :

$$\int_{4\pi} d^2\Omega = 4\pi \tag{1.31}$$

$$\int_{4\pi} d^2\Omega \mathbf{\Omega} = 0 \tag{1.32}$$

The calculation of the term $\int_{4\pi} d^2\Omega \mathbf{\Omega}\mathbf{\Omega}.\mathbf{B}$ can be treated by using the component form of the vectors. As $\mathbf{B}$ is supposed to have no angular dependence, the integration gives two types of terms :

$$\forall i \in \{x, y, z\}, \int_{4\pi} \Omega_i^2 d^2\Omega \tag{1.33}$$

and

$$\forall (i, j) \in \{x, y, z\}, i \neq j, \int_{4\pi} \Omega_i \Omega_j d^2\Omega \tag{1.34}$$

These terms can be computed using spherical co-ordinates. The exact calculation is not showed in this document, but can be found in many reactor physics documents [6]. We obtain:

$$\int_{4\pi} \Omega_x^2 d^2\Omega = \int_{4\pi} \Omega_y^2 d^2\Omega = \int_{4\pi} \Omega_z^2 d^2\Omega = \frac{4\pi}{3} \tag{1.35}$$

and

$$\int_{4\pi} \Omega_x \Omega_y d^2\Omega = \int_{4\pi} \Omega_x \Omega_z d^2\Omega = \int_{4\pi} \Omega_y \Omega_z d^2\Omega = 0 \tag{1.36}$$

Finally, the integrated current can be expressed as function of $\mathbf{B}_g(\mathbf{r})$. Hence, we can obtain the diffusion approximation, also called the P_1 approximation:

$$\phi_g(\mathbf{r}, \mathbf{\Omega}) \simeq \frac{1}{4\pi}[\phi_g(\mathbf{r}) + 3\mathbf{\Omega}.\mathbf{J}_g(\mathbf{r})] \tag{1.37}$$

If we make additional approximations, such as source isotropy, we can obtain Fick's law [6]. This law translates the fact that neutrons migrate from high-density regions towards low density regions. It gives a direct relationship between the neutron current and the flux gradient. The proportionality coefficient D_g is called the diffusion coefficient.

$$\mathbf{J}_g(\mathbf{r}) = -D_g(\mathbf{r})\nabla\phi_g(\mathbf{r}) \tag{1.38}$$

To obtain the diffusion equation, we introduce Fick's law into the transport equation. The diffusion equation is then written :

$$-\nabla.D_g(\mathbf{r})\nabla\phi_g(\mathbf{r}) + \Sigma_g(\mathbf{r})\phi_g(\mathbf{r}) = Q_g(\mathbf{r}) \tag{1.39}$$

1.2 Presentation of the depletion equations

During the reactor operational time, the neutron flux provokes a modification in nuclear properties. Isotopes, such as fission products and actinides, are created. The isotopic densities of isotopes already present in the fuel are also modified. As a consequence, the macroscopic cross sections of the regions are modified. For each isotope i and reaction x the macroscopic cross sections are computed according to formula 1.6.

In turn, the modification of the macroscopic cross sections produces a change in the neutron flux. A burnup calculation consists in an iterative process between depletion step and flux calculation step. The way the isotopes deplete is fully described by the Bateman equations. The methodology implemented in the DRAGON module of evolution `EVO:` is now described.

A nucleus can either be created or disappear. Two different phenomena can provoke the disappearance of a nucleus. First, a nucleus can decay. This reaction is characterized by a radioactive decay constant λ which represents the probability that the nucleus will decay. A second cause of isotopic depletion is a neutron-induced reaction. A neutron-induced reaction does not necessarily lead to the modification of the number of protons and/or neutrons of the isotope. For instance, elastic and inelastic scattering is not a cause of isotopic depletion. All other types of reactions cause isotopic depletion. These reactions are considered in the absorption cross section of an isotope k, given in term of total, elastic and inelastic scattering:

$$\sigma_a(u) = \sigma(u) - \sigma_e(u) - \sigma_{in}(u) \tag{1.40}$$

The absorption cross section is therefore required to compute the isotopic depletion. The loss rate $L_k(t)$ of an isotope k is :

$$L_k(t) = (\lambda_k + \langle \sigma_{a,k}(t)\phi(t) \rangle) N_k(t) \tag{1.41}$$

where
- $\lambda_k(t)$ is the radioactive decay constant for isotope k
- $\sigma_{a,k}(t)$ is the absorption microscopic cross section for isotope k
- $N_k(t)$ is the isotopic density for isotope k

The reaction rates for each reaction x are computed with the formula 1.42 .

$$\langle \sigma_{x,l}(t)\phi(t) \rangle = \int_0^{+\infty} \sigma_{x,l}(u)\phi(t,u)du \tag{1.42}$$

An isotope k can be created according to different reactions :

- An isotope l decays to give birth to an isotope k
- An isotope l undergoes a reaction x to create an isotope k
- An isotope l undergoes a fission reaction to produce an isotope k

When an isotope l undergoes a fission, it can create different fission products. The fission yield Y_{kl} is the number used to take into account the probability that the fission of isotope l gives birth to an isotope k. Finally, we can write the source term of the depletion equation:

$$S_k(t) = \sum_{l=1}^{L} Y_{kl} \langle \sigma_{f,l}(t)\phi(t) \rangle N_l(t) + \sum_{l=1}^{K} m_{kl}(t) N_l(t) \tag{1.43}$$

where

- K is the number of depleting isotopes
- L is the number of fissile isotopes producing fission products
- Y_{kl} is the fission yield for production of isotope k by fissile isotope l
- $m_{kl}(t)$ is the radioactive decay constant or reaction rate for production (other than fission) of isotope k by isotope l

According to the previous considerations, we can write the depletion equations for each depleting isotope, using the equations 1.41 and 1.43 :

$$\frac{dN_k}{dt} + L_k(t) = S_k(t) \text{ with } k \in \{1, .., K\} \tag{1.44}$$

Equations 1.44 forms a set of K linear differential equations. The system can be solved to compute isotopic densities after a time step. However, these equations are dependent on the neutron flux, which in turn depends on the isotopic densities. Generally, the variation of isotopic densities is sufficiently slow. Hence, we can use the adiabatic approximation, which consists in using the solution of the steady-state transport equation. This approximation is no longer valid, for example, when we study transient effects due to the movement of a reactivity device.

Numerical methods can be applied to solve the previous system of differential equations. For certain isotopes, we can also use models such as the saturation model to optimize the calculations.

1.3 `EVO:` power normalization

Two numerical algorithms are implemented in `EVO:` to solve the depletion equations. The depletion system can be solver using either a fifth order Cash-Karp algorithm or a fourth order Kaps-Rentrop algorithm. Here, we choose to use the fourth order Kaps-Rentrop algorithm.

The solution of burnup equations is affected by the flux normalization factors. Two different normalization techniques are implemented: constant flux or constant power depletion. In this work, a constant power depletion is performed. In this case, the power released per initial heavy element at beginning-of-stage and end-of-stage is set to a constant W [9].

$$\sum_{k=1}^{L} \left[\kappa_{\mathrm{f},k} \ \langle \sigma_{\mathrm{f},k}(t_0)\phi(t_0)\rangle + \kappa_{\gamma,k} \ \langle \sigma_{\gamma,k}(t_0)\phi(t_0)\rangle\right] \ N_k(t_0) =$$

$$\sum_{k=1}^{L} \left[\kappa_{\mathrm{f},k} \ \langle \sigma_{\mathrm{f},k}(t_f)\phi(t_f)\rangle + \kappa_{\gamma,k} \ \langle \sigma_{\gamma,k}(t_f)\phi(t_f)\rangle\right] \ N_k(t_f) = C_0 \ W$$

where

- $\kappa_{\mathrm{f},k}$ is the energy (MeV) released per fission of the fissile isotope k ;
- $\kappa_{\gamma,k}$ is the energy (MeV) released per radiative capture of isotope k ;
- C_0 is the conversion factor (MeV/MW) multiplied by the mass of initial heavy elements expressed in metric tonnes.

The end-of-stage power is function of the number densities $N_k(t_f)$; a few iterations are therefore required before the end-of-stage power released can be set equal to the desired value. It should be noted that there is no warranties that the power released keep its desired value at every time during the stage; only the beginning-of-stage and end-of-stage are set.

CHAPTER 2

IMPLEMENTATION OF THE MICRO-DEPLETION METHOD

The work done in this master thesis was performed with the lattice code DRAGON Version4 [9], and the full-core diffusion code DONJON Version4 [10]. Those two codes are part of the Version4 distribution. This distribution is composed of GANLIB (API called by the different components of the distribution [11]), UTILIB (Utility modules), TRIVAC (Full-core flux solver in 1D/2D/3D [12]), DONJON (Environment for full-core calculations), OPTEX (Environment for time-averaged calculations [13]) and DRAGON (Lattice code used for transport studies).

2.1 Introduction to full-core calculation schemes

Reactor core calculation is a two-level computational scheme. The first level is the lattice calculation used to create a cross-section database. A component of the lattice code is dedicated to build the reactor database. It aims to store all the nuclear data produced in the lattice calculations. A finite number of lattice calculations are performed. The results are recorded as function of global and/or local parameters. Typical parameters are :

- burnup or neutron exposure
- fuel temperature
- moderator or coolant temperature
- moderator or coolant density
- poison load
- moderator purity

The second level is the DONJON calculation. In this step, the geometry of the core is composed of homogenized cells, and the condensed properties are recovered from the database, as described in Figure 2.1.

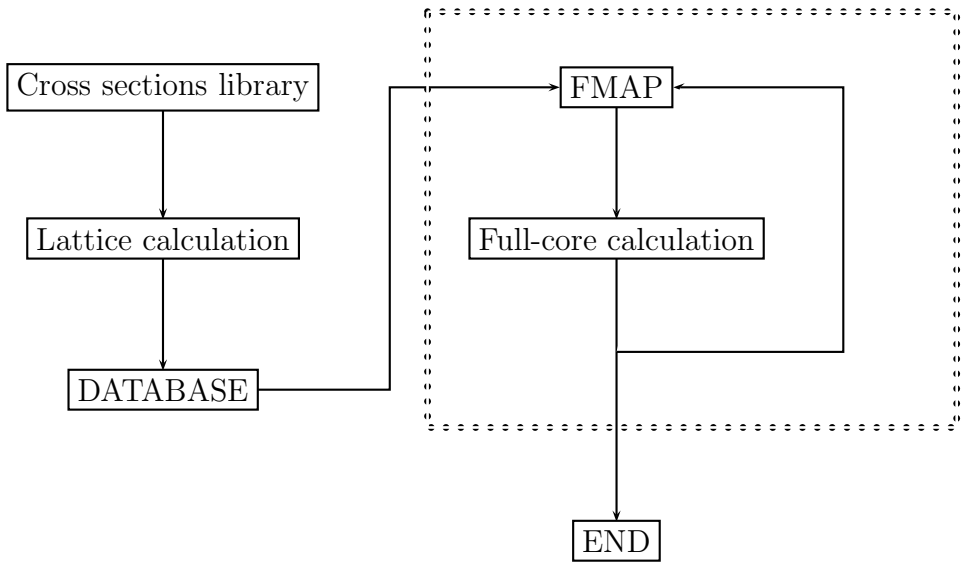

Figure 2.1 Representation of a full-core calculation scheme

The content of the dotted box differs according to the type of calculations. Two types of calculations are introduced thereafter: time-instantaneous calculations using interpolated properties, and microscopic depletion calculations. The global process is to compute fluxes and powers and to update the burnups. The new burnups are available for a new calculation.

In this representation, we have to specify the contents of the objects called DATABASE and FMAP :

- The DATABASE contains the useful nuclear data for the core calculation. The lattice code (DRAGON in our case) has the capability to generate fuel properties at different time step. DRAGON code allows us to have multi-parameter databases. Throughout this document, only mono-parameter databases are considered. The single parameter is the burnup, which represent the depletion of the fuel. Its value is given in energy generated per unit mass (in MWj/t).
- The FMAP is a DONJON object that contains the set of global and local parameters for each bundle in the core. In our case, it contains only the burnup. The FMAP makes the link between the DATABASE and DONJON and creates a new library of microscopic cross sections containing different properties for each bundle, given the burnups of the bundles.

2.2 Presentation of the process

In this section, a presentation of the micro-depletion calculation scheme is provided. First, we introduce the current calculation scheme used to perform time-instantaneous simulations. Then, the new DONJON micro-depletion calculation scheme is presented, as implemented in the code DONJON.

2.2.1 Time-instantaneous calculations with DONJON

The current way to perform a depletion calculation is to interpolate the database at each burnup step and to recover the properties generated by the lattice code. The classic DONJON time-instantaneous calculation scheme is described in the Figure 2.2.

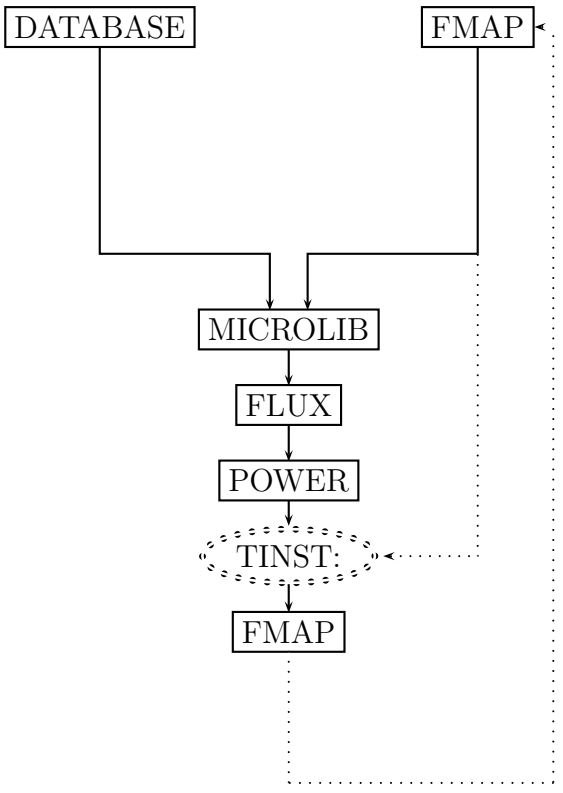

Figure 2.2 DONJON time-instantaneous calculation scheme

The module `TINST:` is the central module when a time-instantaneous calculation is performed. In Figure 2.2, we have not displayed all the modules used in DONJON and TRIVAC to solve the diffusion equation, and to compute the fluxes and powers in each bundle. The object named POWER is a L_POWER object as described in the technical report [9], contains

the information on powers in the whole core. The FMAP contains the burnup information. The call to `TINST:` is required to calculate the new burnup distribution, according to the bundle powers and the previous burnups. The formula 2.1 sums up the role of the module `TINST:`.

$$B_{i,j}(t + \Delta t) = B_{i,j}(t) + \frac{P_{i,j}(t)\Delta t}{m_{i,j}(t)} \tag{2.1}$$

where

- i is the number of the fuel channel
- j is the number of the bundle in the fuel channel
- Δt is the step time chosen by the user of the module
- $B_{i,j}(t)$ is the burnup in fuel channel i and bundle j
- $P_{i,j}(t)$ is the power in fuel channel i and bundle j
- $m_{i,j}(t)$ is the mass of initial heavy elements in channel i and bundle j

After the call to the `TINST:` module, the new burnups are computed and stored in the FMAP object. A new interpolation in the DATABASE can therefore be done for a new step of calculation.

We can notice here the dependence of the full-core calculation to the lattice code. At each time step, we have to interpolate the properties of the different fuels in the database, previously generated by the lattice code.

The goal of this work is to replace the `TINST:` module with a depletion module, used to solve the depletion equations. Solving the depletion equations in a full-core calculation is called microscopic depletion. Such a module is already programmed in DRAGON, called `EVO:`. As a first step, we have to implement this module in the DONJON environment, and perform simple micro-depletion calculations using flux distributions from the TRIVAC diffusion solver. This is the subject of Chapter 3, where simple Benchmarks are studied, on fuel assemblies. Then, the goal is to be able to deplete a whole core of CANDU-6, with all its features. Finally, an important capability for new reactors is to be able to deplete different fuel rings and pins of a cell in a core calculation.

2.2.2 Micro-depletion calculations with DONJON

The depletion module of DRAGON `EVO:` is going to be implemented in DONJON to be used for micro-depletion calculations. The goal is to solve the depletion equations for each

homogenized region, using a flux coming from the diffusion code TRIVAC. At each time step, `EVO:` updates the macroscopic cross sections, and creates a new library of microscopic cross sections. The scheme 2.3 represents the mechanism of micro-depletion, which can be compared with Figure 2.2.

In this type of calculation, burnup steps are performed with `EVO:`. After the call to the depletion solver, isotopic densities are updated. The database is no longer used to recover the concentrations. Actually, as will be explained later in this document, a mixed method is implemented using both an interpolation and a micro-depletion calculation. A combination of the two methods allows both to save computational time and to get more accurate results.

Figure 2.3 gave the general mechanism of the micro-depletion calculation scheme. A closer study of the way the depletion solver is implemented in DONJON is provided in the next subsection.

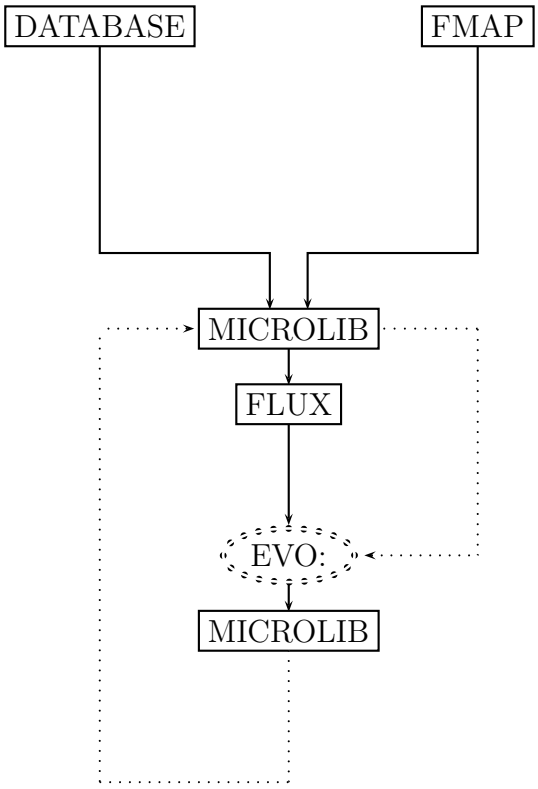

Figure 2.3 General DONJON micro-depletion calculation scheme

2.3 Data flow diagrams

In this subsection, the data flow diagrams of DRAGON and DONJON micro-depletion calculation schemes are given. The names of modules or data structures are not necessarily those used in the technical reports [9] [14] [10]. The diagrams are simplified to emphasize the existing differences in the two processes. A classic depletion calculation scheme in DRAGON is described in Figure 2.4. The equivalent DONJON calculation is given in Figure 2.5. The description of data structures and modules used is given below.

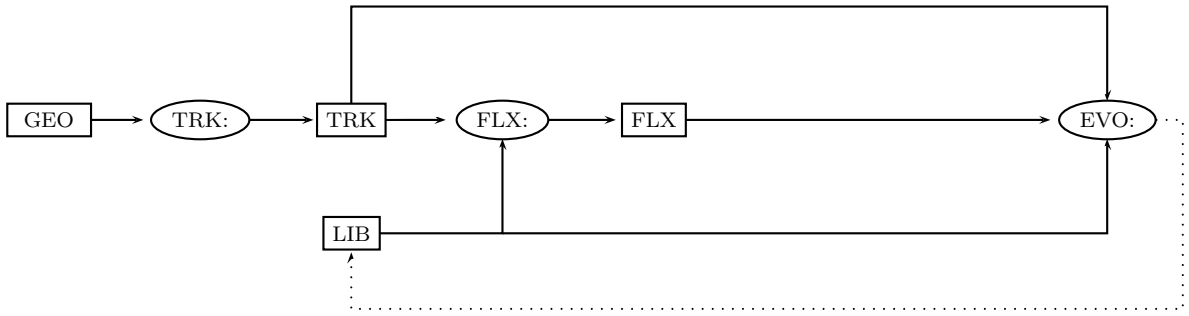

Figure 2.4 Data flow diagram of DRAGON micro-depletion calculation scheme

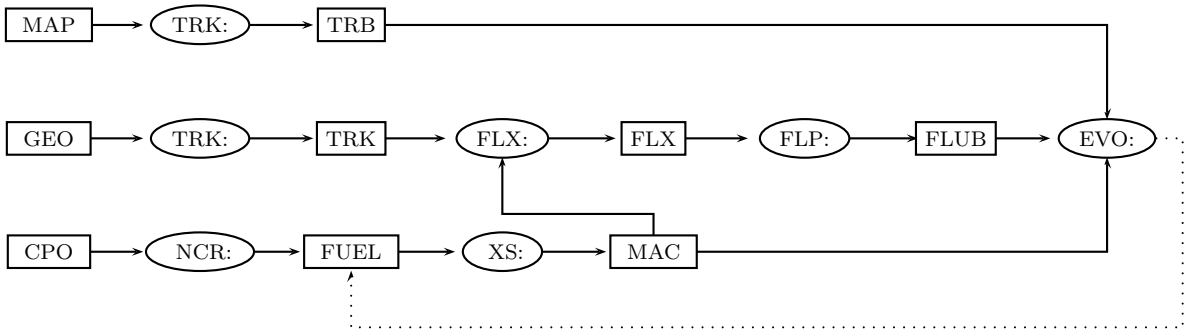

Figure 2.5 Data flow diagram of DONJON micro-depletion calculation scheme

The data structures involved are :

GEO	The geometry to be studied
MAP	The fuel-map geometry
TRK	The results of the geometry tracking
TRB	The results of the fuel-map geometry tracking
FLX	The fluxes over the fine mesh geometry GEO
FLB	The fluxes over the fuel-map geometry MAP
DB	The database containing fuel and reflector properties
LIB	The microscopic cross sections library over the fine mesh geometry GEO
FUEL	The microscopic cross sections library over the fuel-map geometry MAP
MAC	The macroscopic cross sections library over the fine mesh geometry GEO

The modules involved are :

`TRK:`	A tracking module. Several are available.
`FLX:`	A solver for the transport or diffusion equation, according to the method.
`FLP:`	A module used to normalize and compute bundle fluxes.
`EVO:`	The depletion equations solver.
`NCR:`	The module used to interpolate multi-parameter databases.
`XS:`	A combination of DONJON modules to construct a complete macrolib, including reflector properties, and device properties, if needed.

The principle of depletion calculations is to use a depletion equations solver to compute new isotopic densities after each time step. New macroscopic cross sections are computed according to formula 1.6. These cross sections are used to perform a new flux calculation. The neutronic flux allows us to compute the new reaction rates. A new call to `EVO:` can thus be performed, using the updated reaction rates.

The `EVO:` module requires three input files to be able to solve the Bateman equations : the geometry tracking, the fluxes over this geometry, and the corresponding library of microscopic cross sections.

As the DONJON and DRAGON environments are different, differences appear also in the modular sequence called by the two codes. For example, the depletion solver uses different input geometries. In a full-core study, two different geometries are commonly used. First, we have the detailed geometry containing all the regions in the core. This geometry is called

GEO in Figures 2.4 and 2.5. It is a fine mesh geometry that contains the reflector and the device regions. This geometry is used by the flux solver to produce fluxes and powers over the reactor. The GEO geometry is also present in lattice computations and is used by `EVO:` to carry out burnup steps.

A second geometry is required in the DONJON code. An association between the resolution geometry and the bundle definitions is performed via a fuel map object containing a fuel map geometry named MAP (see Figure 2.5). This structure contains a coarser core geometry, defined to encompass the solution domain and thus create a direct link between the meshes and the fuel bundle locations. We use this geometry to register CANDU cell properties, such as burnups or poison loads. It is generally used for full-core studies. In DONJON, this geometry is the one used for the depletion. Other regions, such as reflector materials, are considered as non-depleting regions. It is simpler to perform DONJON micro-depletion calculations over this geometry for several reasons. First, the DONJON code has already the capability to produce a library of microscopic cross sections over the fuel geometry. However, it is not yet possible to include devices and reflector materials in this library. Hence, no significant amount of additional programmation was required. Secondly, the fuel map geometry is well-suited for depletion calculations as only non-splitted fuel cells are included. The micro-depletion is thus performed over a coarse mesh rather than a fine mesh to save computational time.

The diffusion solver of DONJON computes the flux distribution over the mesh corresponding to the first geometry GEO. A special process has to be done so as to input the flux in the `EVO:` module. The flux distribution has to be condensed to produce one flux per fuel cell. This step is carried out by the `FLP:` module (see Figure 2.5).

Other features of the DONJON micro-depletion calculation scheme come out on the above Figures. Special modules are dedicated to the consideration of reflector materials and device materials. These materials are added to the fuel-map library to modify the macroscopic cross sections. Such modules are not present in the DRAGON data flow diagram.

2.4 Homogenized microscopic cross section interpolation

In micro-depletion, we replace the way the fuel depletion is performed. Isotopic concentration computation is therefore carried out solving the depletion equations instead of computing the fuel burnup.

However, isotopic densities are not the only quantities varying when the fuel burns. Microscopic cross sections used in full-core studies are computed during the lattice calculation step. Homogenized cross sections are recovered from lattice calculations. The weight function used to condense the cross sections is the transport flux. As fuel burns, the transport flux changes. Therefore, few groups homogenized cross sections vary. Equations 1.25 and 1.26 show the dependency. To perform accurate micro-depletion calculations, we have to take care of this phenomenon.

The way of proceeding is to recover microscopic cross sections from the database. At each burnup step, interpolation is performed to compute new condensed cross sections while isotopic depletion is made by `EVO:`. Cubic polynomials are used to perform the database burnup interpolation. Additional information concerning the interpolation process as implemented in DRAGON can be found in Reference [9].

CHAPTER 3

ELEMENTS OF VALIDATION OF THE MICRO-DEPLETION METHOD

CANDU reactors consist on a cylindrical calandria filled with heavy water moderator, and penetrated by 380 fuel channels. Each channel is filled with 12 bundles. Depending on their positions and their burnups, the bundles are not exposed to the same fluxes. Therefore, they don't deplete at the same pace. In classic macroscopic depletion calculations, reactor burnup distribution is simulated by solving two-group static diffusion equations at discrete time steps, assuming a constant flux distribution over each interval. In microscopic depletion calculations, fuel depletion is carried out solving Bateman equations.

Generally, a single multi-parameter database is used to perform a full-core calculation. This database is generated at a nominal power in DRAGON. Fuel bundle average fission power is fixed to 615 kW for a CANDU-6 reactor. So, the isotopic densities tabulated in the database are dependent on the power used at the lattice step. However, when we use an interpolation method, the nuclear properties are computed according to the burnups. Certain isotopic densities can thus be biased with this method. Isotopes, such as fission products or actinides, are more dependent on the current power level than on the irradiation of the fuel bundle. Xenon-135 is an important example. This is one of the most important isotope in the reactor operation. Hence, a special DONJON module is dedicated to the correction of Xenon density. This `XENON:` module aims at improving the evaluation of Xenon density. It corrects the interpolated densities. A presentation of this module is done in the next section.

Another crucial point is the choice of isotopes to extract in the micro-depletion process. The more we extract isotopes the more accurate the calculation is, but the more time it takes to perform the simulation. By default, about 250 isotopes are considered, which is not a reasonable number, because it leads to the creation of huge databases. The depletion of a full core requires the selection of a restricted number of isotopes both to save computational time and to reduce the size of the library of microscopic cross sections. This selection results from a compromise. A more reasonable number is to extract between 30 and 50 isotopes for the micro-depletion. The following isotopes are extracted for our micro-depletion calculations:

- 6 heavy nuclides (U-235, U-238, Np-239, Pu isotopes) ;
- 23 fission products (Sm isotopes, Pm isotopes, Eu isotopes, Nd isotopes, Xe-135, Rh-105, Cd-113, Gd-157 and I-135).

The contribution of non-extracted isotopes is represented by a residual isotope. This isotope is non-depleting, and captures the effects of nuclides not modelized in the isotopic chains. The residual isotope density is set to 1.0. Actually, this isotope is defined by a macroscopic cross section Σ^{RES}. For each reaction x and energy group g, we have the following relation :

$$\Sigma_{x,g} = \Sigma_{x,g}^{RES} + \sum_i N_i \sigma_{x,g,i} \tag{3.1}$$

In a micro-depletion calculation scheme, the non-depleting isotopes, such as the residual ones, maintains the same properties during the depletion. However, when a limited number of isotopes is extracted, the influence of the residual isotope is important. The residual macroscopic cross section is altered at each time step. To avoid a large loss of precision, we have to take into account the evolution of the residual properties. The solution is to recover the corresponding nuclear properties from the database, even with a micro-depletion method.

Therefore, we can use a mixed method to be more accurate. The micro-depletion method is coupled with an interpolation calculation. The interpolation is performed at each burnup step both to interpolate the residual properties and to compute the burnup-dependent homogenized microscopic cross sections. This type of calculation can allow to reach almost the same accuracy as a full-extraction calculation. Such a mixed calculation is implemented in DONJON and described in Appendix A, for the Benchmark 2.

The study of a CANDU-6 cell with reflective boundary conditions is a good method to evaluate the impact of different parameters on a micro-depletion calculation. It is a preliminary level, before performing the simulation of a full core. Two different Benchmarks are studied in this Chapter, with different methods of calculations. An accurate description of each calculation is given in each Benchmark subsection. The two Benchmarks are :

- Benchmark 1 : A single fuel cell of CANDU-6 with reflective boundary conditions.
- Benchmark 2 : An heterogenous assembly composed of 36 fuel cells. The boundary conditions are reflective.

3.1 The XENON: module

Xenon-135 is an important isotope in a reactor, because it has a large capture cross section. An error in the computation of the Xenon-135 concentration can cause a noticeable modification of the core reactivity. During an interpolation calculation, the Xenon concentration is recovered from the database. This database is generally parameterized in burnup (or an other parameter representative of the irradiation of the fuel). This way of proceeding tends to bias the evaluation of the Xenon density. This isotope is dependent on the flux rather than on the burnup. This phenomenon can be pointed out on other fission products.

To improve the calculation of the Xenon distribution, a special module was implemented in the DONJON code. This module has been exclusively developed for the need of this project. The implantation of the module in the classic calculation scheme requires a particular routine. A recursive call to the XENON: module is done to converge on the static distribution of Xenon.

3.1.1 Saturated concentration of Xenon-135

Xenon-135 has a decay constant corresponding to a half-life of $T_X = 9.17h$. The study of the depletion equations of Xenon-135 and Iodine-135 leads to conclude that, after a few days, if we consider a constant flux, the Xenon-135 isotope reaches an equilibrium, given by the following equation [15]:

$$N_{X_{eq}} = \frac{(Y_I + Y_X)\Sigma_f \phi}{\lambda_X + \sigma_X \phi} \tag{3.2}$$

where

- Y_I is the fission yield of Iodine-135
- Y_X is the fission yield of Xenon-135
- σ_X is the capture cross section of Xenon-135
- λ_X is the decay constant of Xenon-135
- Σ_f is the total fission cross section
- ϕ is the fuel cell flux

As a consequence, the equilibrium concentration of Xenon-135 is only dependent of the flux level in the region. Figure 3.1 gives the dependence of the Xenon-135 equilibrium density with the neutronic flux.

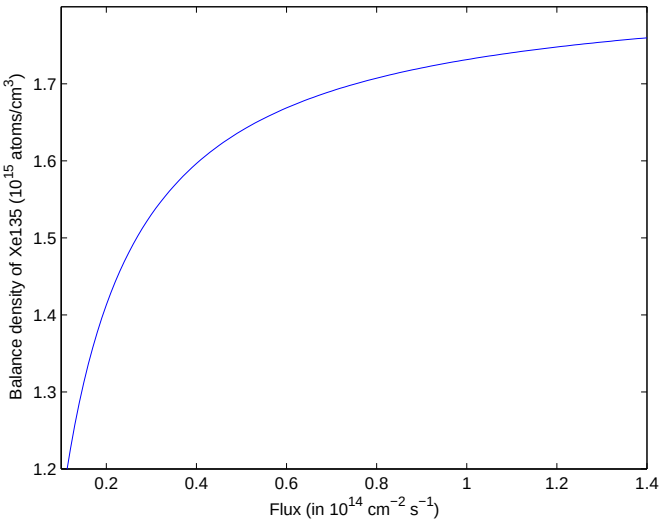

Figure 3.1 Xenon-135 equilibrium density as a function of flux

3.1.2 Procedure for Xenon calculations

The correction of Xenon concentrations is performed using an iterative routine. This iterative procedure requires an initialization of the Xenon-135 distribution. The choice is to set Xenon densities to zero. This is not problematic for the convergence. About 3 iterations are required for a criterion of 1 mk.

First of all, a flux calculation is performed without the presence of Xenon in the microscopic cross section library. Xenon-135 equilibrium concentrations are thus computed, according to Equation 3.2. The new concentrations are added to the old library, and new macroscopic cross sections are computed.

These new cross sections are used for a new flux calculation, which, in turn, gives a new static distribution of Xenon-135. A criterion is set to stop the loop. When the k_{eff} has converged, we obtain the final distribution. This process is summarized in the following Figure.

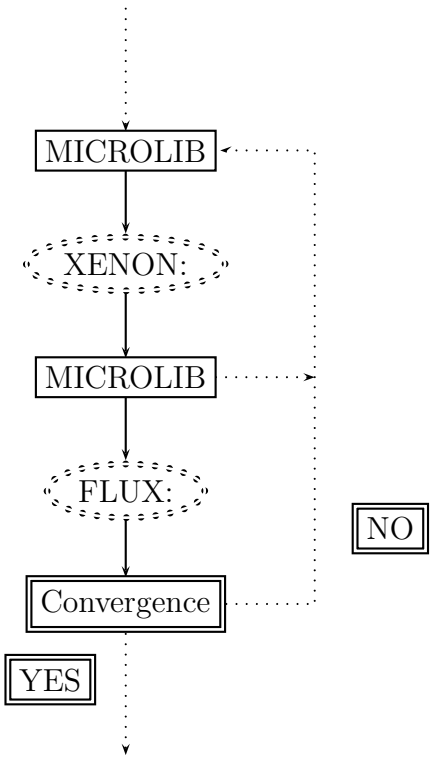

Figure 3.2 Calculation scheme with the `XENON:` module

3.2 Benchmark 1 : CANDU-6 fuel cell depletion

To test the ability of the DONJON code to perform microscopic depletion calculations, a simple geometry is simulated. The depletion of a fuel cell with reflective boundary conditions is investigated in the following section.

3.2.1 Description of the case

To compare and evaluate our micro-depletion calculation, a DRAGON reference is used. The DRAGON computation is made on an accurate CANDU-6 geometry, as described in Figure 3.3. This simulation is performed with a 172-groups JEFF2.2 DRAGLIB. Heavy isotope cross sections are corrected by self shielding approach. The cell volumes are tracked to be able to compute collision probability matrices. The simulation is a fission source eigenvalue problem, where the eigenvalue is the effective multiplication factor (type K). A 150 day depletion is carried out.

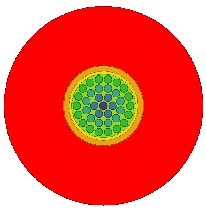

Figure 3.3 Benchmark 1: Geometry for transport calculations

The CANDU-6 fuel cell is composed of :

- The coolant zone located at the center of the cell.
- 37 fuel pins, each one surrounded by a ring made of zirconium, and located in the coolant zone.
- The pressure tube made of Niobium and Zirconium.
- The helium gap.
- The calendria tube made of Zirconium.
- The moderator zone which fills about 80% of the cell.

The DONJON calculations are made on a homogenized geometry, with 2-groups properties. Geometry of Benchmark 1 is represented on Figure 3.4. The DONJON code is based on the TRIVAC multigroup diffusion solver [12]. A mesh-centered finite difference method is used

to compute the fluxes. For the micro-depletion method, a set of 29 isotopes is extracted and compared to a full extraction calculation.

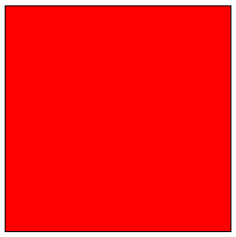

Figure 3.4 Benchmark 1: Geometry for diffusion calculations

The reactor database is generated at a nominal power of 31.9713 kW/kg, which is the fuel bundle average power in a CANDU core. To evaluate the impact of power normalization on isotopic concentrations, four different calculations are made for each case. The four cases correspond to :

- A simulation at 10% of the nominal power.
- A simulation at 50% of the nominal power.
- A simulation at 100% of the nominal power.
- A simulation at 140% of the nominal power.

For each power, five different computations are studied. The acronyms prior to the description are the one used for the results analysis (tables, curves) :

- `DRAGON` : A classical DRAGON calculation where the depletion of the fuel is performed by the module `EVO:`.
- `DONJON` : A DONJON micro-depletion calculation where the depletion of the fuel is performed by the DRAGON module `EVO:`, as depicted in Figure 2.3. A limited selection of isotopes is considered for solving the depletion equations. Interpolation is realized both to compute residual properties and burnup-dependent homogenized microscopic cross sections.
- `DONALL` : A DONJON micro-depletion calculation where the depletion of the fuel is performed by the DRAGON module `EVO:`, as depicted in Figure 2.3. All the available isotopes are considered for solving the depletion equations.
- `TINST` : A DONJON calculation where the depletion of the fuel is performed by the `TINST:` module, as depicted in Figure 2.2.

- `XENON` : A DONJON calculation where the depletion of the fuel is performed by the `TINST:` module, as depicted in Figure 2.2. The `XENON:` module is used to take care of distributed Xenon effects.

3.2.2 Results

On Figure 3.5, the k_{eff} is plotted in function of time for each power. The k_{eff} deviation after 150 days is given in tables 3.1, 3.2, 3.3 and 3.4. It is defined in reference to the DRAGON calculation, as specified by the formula below:

$$\Delta k_{eff} = 10^3 \times (k_{eff} - k_{eff}^{REF}) \tag{3.3}$$

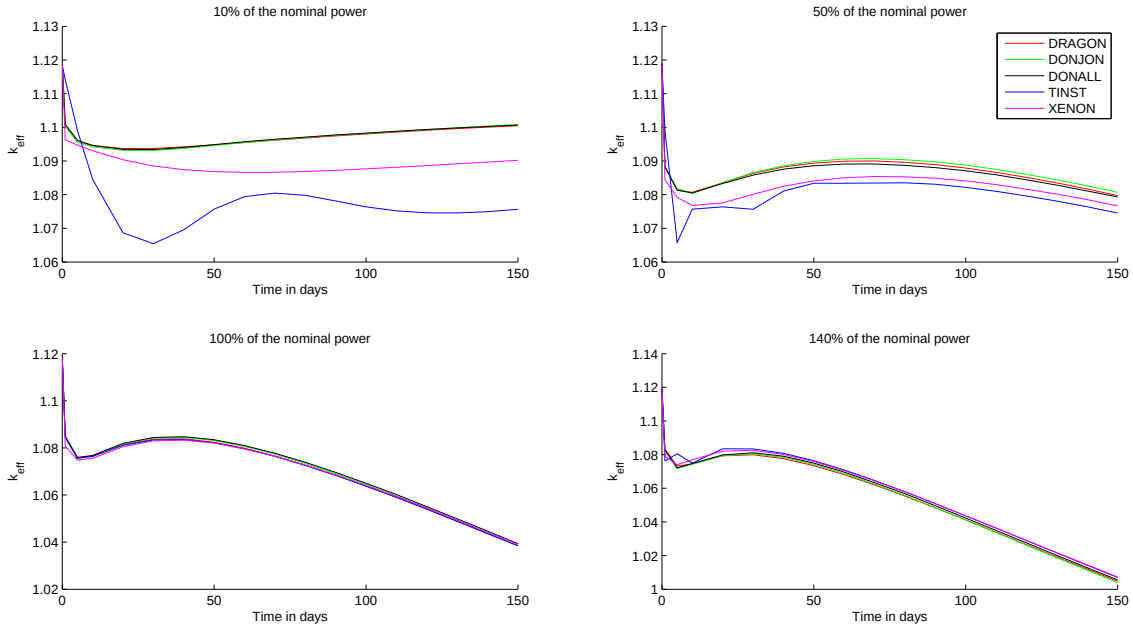

Figure 3.5 Benchmark 1 : Effective multiplication factor for four cases of power

Table 3.1 Benchmark 1: Multiplication factor after 150 days for $\frac{P}{P_{ref}} = 1.4$

Method	k_{eff}	Δk_{eff} in mk
DRAGON	1.004775	/
DONJON	1.003978	-0.7970
DONALL	1.005539	0.7640
TINST	1.006983	2.2079
XENON	1.007289	2.5140

Table 3.2 Benchmark 1: Multiplication factor after 150 days for $\frac{P}{P_{ref}} = 1$

Method	k_{eff}	Δk_{eff} in mk
DRAGON	1.038494	/
DONJON	1.038624	0.1300
DONALL	1.039377	0.8830
TINST	1.038418	-0.0759
XENON	1.039021	0.5269

Table 3.3 Benchmark 1: Multiplication factor after 150 days for $\frac{P}{P_{ref}} = 0.5$

Method	k_{eff}	Δk_{eff} in mk
DRAGON	1.079732	/
DONJON	1.080678	0.9460
DONALL	1.0793310	-0.4010
TINST	1.074543	-5.1889
XENON	1.076675	-3.0569

Table 3.4 Benchmark 1: Multiplication factor after 150 days for $\frac{P}{P_{ref}} = 0.1$

Method	k_{eff}	Δk_{eff} in mk
DRAGON	1.100485	/
DONJON	1.100849	0.3640
DONALL	1.100691	0.2060
TINST	1.075661	-24.8239
XENON	1.007289	-10.2679

For a fuel cell at nominal conditions, the calculation based on interpolation is very accurate. The properties used are recovered from a DRAGON calculation at each time step. As this calculation is made at the same power, the `TINST:` method is very consistent with the DRAGON reference. The micro-depletion gives also good results at this power. However, the deviation is a little higher than a `TINST:` method. This error is due to the fact that the DONJON calculation is done with a simplified model, in comparison to DRAGON. We use homogenized and condensed properties, and the diffusion approximation to perform the DONJON micro-depletion calculation. Hence, the isotopic densities are updated using diffusion reaction rates.

The numerical results show that using a mixed method makes up for the loss of precision due to a restricted extraction. A deviation of about 0.13 mk is present, after 150 days. This difference reaches 0.36 mk for low powers. The study is done for an extraction of 29 isotopes, in comparison to about 250 isotopes. The benefits in computational time are huge. The computational time is reduced by almost a factor 10. For high powers, the mixed method is even more precise than the full extraction calculation. The deviation is reduced from 0.88 mk to 0.13 mk. This method uses interpolated properties for the non-extracted isotopes. As the interpolation is very precise at nominal conditions (a deviation of 0.07 mk), it improves the results for the `DONJON` case. Hence, this method is a very good compromise between accuracy and computational time.

For a fuel cell at low power, the conclusions are inverted. The micro-depletion method seems to be more consistent with the reference calculation. Once more, the mixed scheme using both the interpolation and micro-depletion schemes turns out to be very efficient. This time, the Δk_{eff} is a little higher when we use this method than using a strict micro-depletion. However, the numerical results are good for both. Respectively, there is a deviation of 0.9 mk and 0.4 mk for P=0.5 and of 0.36 mk and 0.20 mk for P=0.1.

For low powers, the results are much less realistic when an interpolation method is used. The multiplication factor obtained at the end of the simulation period is around 25 mk lower than the DRAGON reference. Several isotopes have a density related to the power level in the bundle. However, the density recovered from the database is the one corresponding to nominal conditions. Basically, the Xenon concentration is the saturated concentration corresponding to the fuel bundle average power. So this phenomenon can create an underestimation of the reactivity. One also notices the improvement in the results when the `XENON:` module is added. It provides a 14 mk gain for $0.1 \times P_{nom}$. For 50% of the power, the bias is reduced from 5 to 3 mk. However, it turns out to be less accurate for the nominal power.

To understand the power effects, the density of Xenon-135 is plotted in Figure 3.6 for the different powers and methods. This isotope has a density dependent on the flux level and is representative of this phenomenon.

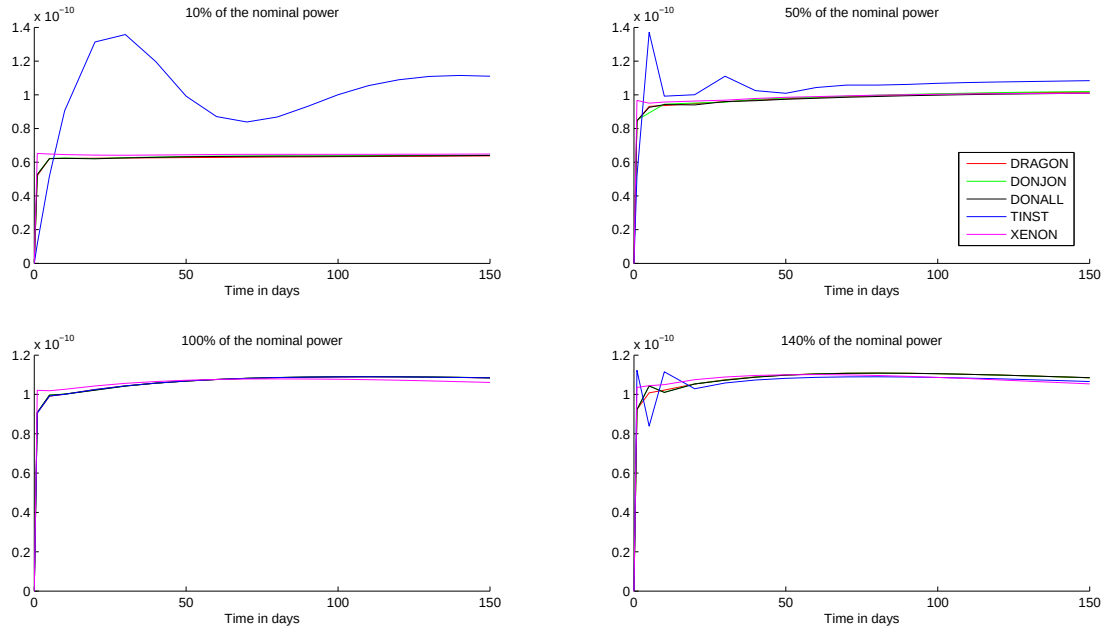

Figure 3.6 Benchmark 1 : Xenon-135 density for four cases of power

For lower power depletions, we can see that the density is overestimated by the interpolation method. This can explain the fact that k_{eff} is smaller than the reference in this case. This phenomenon is more pronounced at 10% of nominal conditions than at 50%.

The micro-depletion method allows us to get a concentration more representative of the real depletion of the fuel than an interpolation method. The concentration is consistent with the value of the flux. The correction of the Xenon distribution is a good mean to get better results in a macro-depletion calculation.

This Xenon effect is expected to be more striking on a full core, as many fuel cells are far from nominal conditions. The shape of the flux and Equation 3.2 imply that peripheral fuel cells should have a low Xenon-135 concentration with a micro-depletion method. This is more accurate than using the nominal power saturated concentration.

Uranium-235 densities are plotted in Figure 3.7.

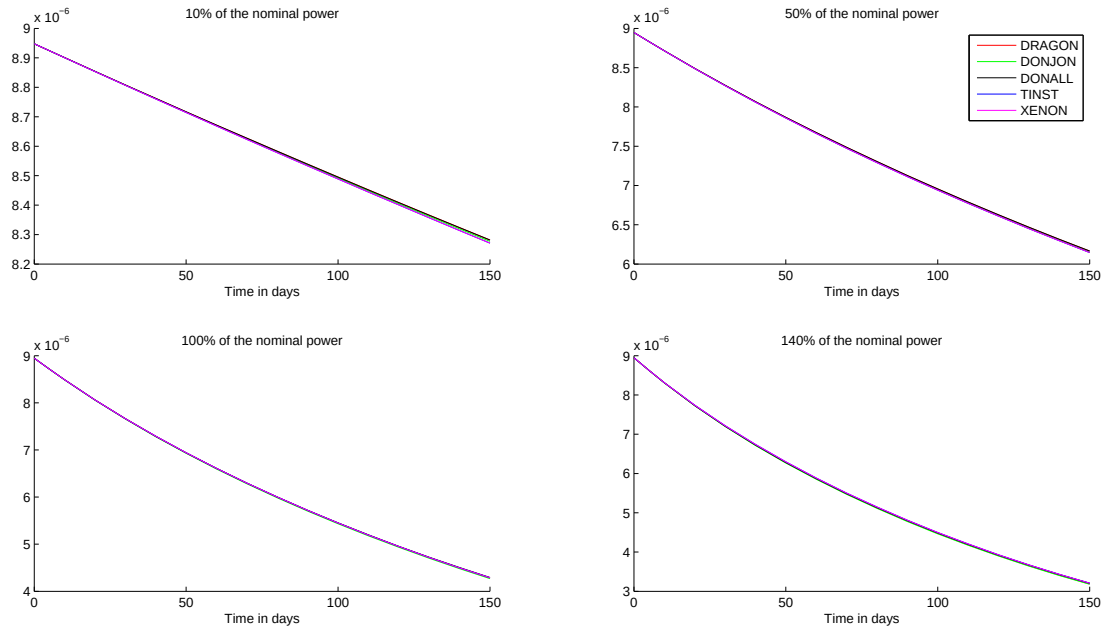

Figure 3.7 Benchmark 1 : Uranium-235 density for four cases of power

The evaluation of Uranium-235 is very good, regardless of the method used. Uranium-235 density depends mostly on the bundle burnup. So power effects have no impact on the computation of the Uranium-235 density. The micro-depletion method is also very consistent with the DRAGON reference.

3.2.3 Conclusions

The study of the previous simulations allows to reach the following conclusions :

- For nominal conditions, the interpolation method is more precise than a micro-depletion calculation. The properties used in this case are coming from an accurate transport calculations. The micro-depletion shows also a good concordance with DRAGON (less than 1 mk of error).
- A limitation of the interpolation is the estimation of fission products. For bundles depleting at low powers, the evaluation of certain fission products, such as Xenon-135, is biased. So, k_{eff} is under evaluated. A solution would be to generate different databases at different power levels, and to recover the corresponding nuclear properties, according to the local power. A simpler solution is to use a module to take care exclusively of Xenon-135, which is the main responsible for the discrepancy.
- The iterative procedure used to correct the Xenon concentration is a good mean to improve our results. Also, it does not require significant additional computational time. Obtaining the solution of the diffusion equation takes only a few seconds on a whole CANDU-6 reactor.
- The loss of precision due to the limited extraction of isotopes is well compensated by the interpolation of the residual properties. The related calculation scheme gets more complicated, but the results are accurate. Moreover, the amount of additional computation time due to interpolation is largely compensated by the fact that we can decrease the number of extracted isotopes. Only important fission products and actinides need to be considered.
- The mixed procedure for micro-depletion benefits from the advantages of both methods. The interpolation of residual properties is very accurate at nominal conditions. For low powers, it is a little biased in comparison to a full extraction. A solution would be to extract additional isotopes.

3.3 Benchmark 2: CANDU-6 fuel assembly depletion

3.3.1 Description of the case

To evaluate the micro-depletion method, our second Benchmark is made on a more complicated assembly of fuel cells. CANDU-6 fuel cells are included in a 6 by 6 assembly (see Figure 3.8). The cells are already homogenized and no detailed geometry is used in this Benchmark. Initially, 32 fuel bundles (in blue) are fresh bundles. The four others located at the right lower-corner (in red) have an initial burnup of 8000.0 MWj/t.

A reference calculation is performed using a transport solver. The collision probability method is used. All the other calculations are performed using a flux solver for the diffusion equation. A mesh-centered finite difference is used. Geometry for Benchmark 2 is described in Figure 3.8. The transport calculation is executed through the DONJON environment. Actually, the solver for the probability collision is added to the DONJON environment to perform the micro-depletion reference case. The diffusion calculations are performed on a three-dimensional Cartesian geometry. The boundary conditions associated with the different surfaces are reflective.

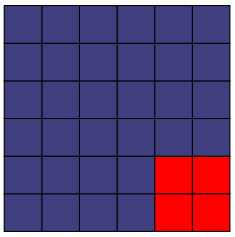

Figure 3.8 Benchmark 2: Geometry

The power distribution is computed at the initial time. The result is shown in Figure 3.9. The power variation over the assembly is important. This study aims to illustrate the impact of the power value on the isotopic concentration calculation.

In this Benchmark, four different calculations were considered. The acronyms prior to the case description are the one used for the result analysis (tables, curves) :

- `DRAGON` : A classical DRAGON calculation where the depletion of the fuel is performed by the module `EVO:`.
- `DONJON` : A DONJON micro-depletion calculation where the depletion of the fuel is performed by the DRAGON module `EVO:`, as depicted in Figure 2.3. A limited selection

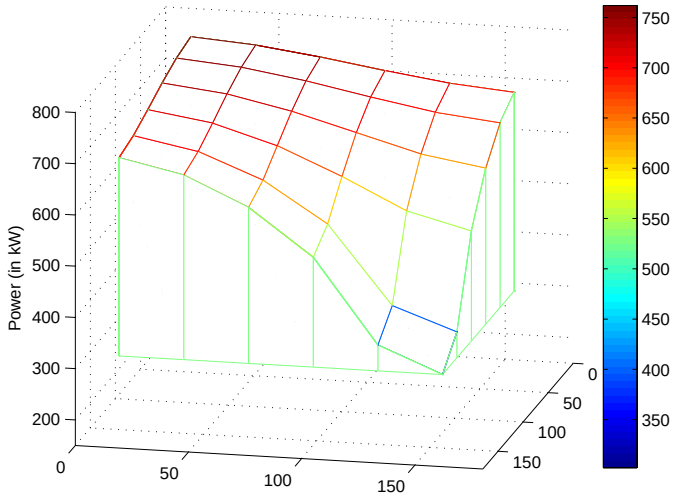

Figure 3.9 Benchmark 2: Power distribution at initial time

of isotopes is considered for solving the depletion equations. Interpolation is realized both to compute residual properties and burnup-dependent homogenized microscopic cross sections.

- `TINST` : A DONJON calculation where the depletion of the fuel is performed by the `TINST:` module, as depicted in Figure 2.2.
- `XENON` : A DONJON calculation where the depletion of the fuel is performed by the `TINST:` module, as depicted in Figure 2.2. The `XENON:` module is used to take care of distributed Xenon effects.

The calculations were made for two cases. The goal is to underline the impact of local power on the calculations.

– The assembly depletes at a power corresponding to the power used to generate the database (31.97 kW/kg).
– The assembly depletes at a power lower to the power used to generate the database (10 kW/kg).

3.3.2 Results

On Figure 3.10, the effective multiplication factor of the assembly is plotted as function of time for the two powers. The k_{eff} deviation (in mk) after 150 days is given in tables 3.3.2 and 3.3.2. It is defined in reference to the DRAGON calculation, as specified by the formula

below:

$$\Delta k_{eff} = 10^3 \times (k_{eff} - k_{eff}^{REF}) \tag{3.4}$$

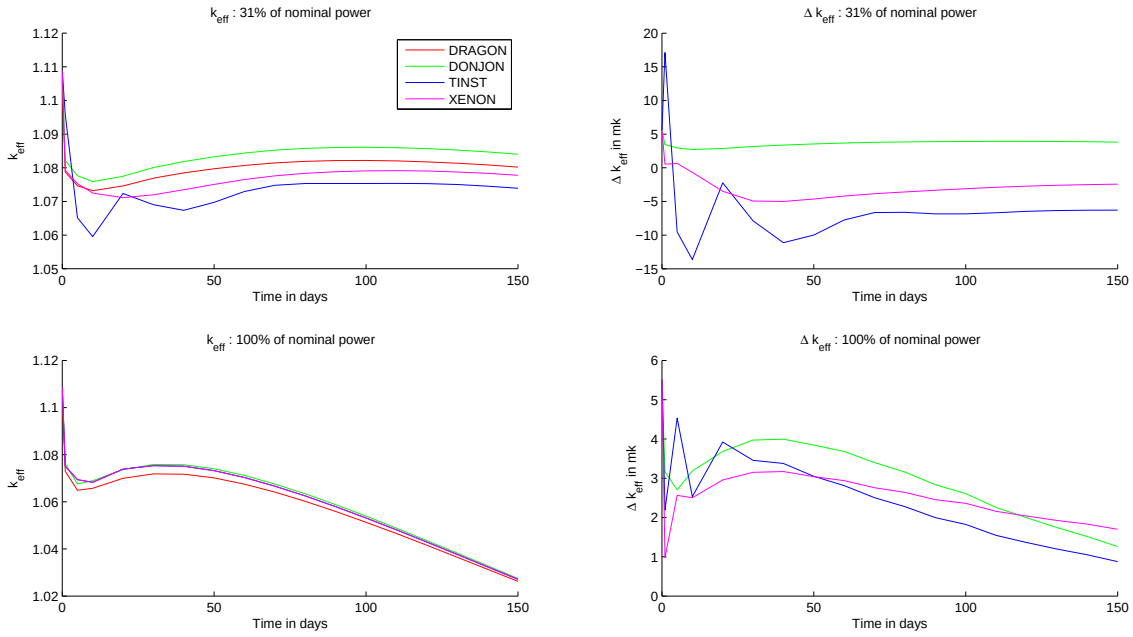

Figure 3.10 Benchmark 2 : Effective multiplication factor for the two calculations

Table 3.5 Benchmark 2: Multiplication factor after 150 days for P=31.97 kW/kg

Method	k_{eff}	Δk_{eff} in mk
DRAGON	1.026215	/
DONJON	1.027474	1.26
TINST	1.027091	0.88
XENON	1.027915	1.70

For nominal conditions, the three calculations have a Δk_{eff} lower to 1.7 mk. One can notice that the interpolation calculation gives better results. The final deviation is lower to 1.26 mk for the micro-depletion. It is reduced to 0.88 mk with the interpolation. In this case, the use of the `XENON:` module does not improve our results, as the quantity of Xenon is well

Table 3.6 Benchmark 2: Multiplication factor after 150 days for P=10.0 kW/kg

Method	k_{eff}	Δk_{eff} in mk
DRAGON	1.080219	/
DONJON	1.084032	3.81
TINST	1.073935	-6.28
XENON	1.077782	-2.44

evaluated by `NCR:`. On the contrary, the approximation made for the calculation of Xenon concentrations tends to bias slightly the multiplication factor.

At 10.0 kW/kg, the reactivity bias is more important with the `TINST:` method. The k_{eff} is under evaluated with this method. The difference is about 7 mk after 150 days of depletion. The use of the Xenon correction allows decreasing the gap from 6.3 to 2.4 mk. We can conclude that, if an important part of the error is coming from the Xenon evaluation, it is not the only responsible. Other isotopic concentrations have to be biased by the interpolation process. It does not seem to be the case for Uranium-235, which is well computed by all the solvers. Uranium-235 average density is plotted in Figure 3.11. The isotopic concentrations of Xenon-135, Samarium-149 or Plutonium-239 are plotted thereafter. Fuel cell average densities are plotted in Figure 3.12, 3.13 and 3.14.

We observe large oscillations of the Xenon concentration when interpolation is used. Normally, the concentration becomes stable after a few days. Here, it requires about 50 days to reach a balance state. This is due to the fact that the calculation of the concentration is done according to the bundle burnup. As the burnup increases slowly, it takes more time to become stable. The relative error on Xenon-135 density is reduced by a factor 10 using the Xenon correction module. So, it improves considerably the results as compared to the interpolation calculation. The case of the Samarium-149 is different. A big difference in comparison to Xenon-135 is the fact that the balance concentration of Samarium-149 is not power-dependent. The study of the depletion equations of Samarium-149 and Promethium-149 leads to conclude that, after a few days, the Samarium-149 isotope reaches an equilibrium, given by the following equation [15]:

$$N_{S_{eq}} = \frac{Y_S \Sigma_f}{\sigma_S} \tag{3.5}$$

where

– Y_S is the fission yield of Samarium-149

- σ_S is the capture cross section of Samarium-149
- Σ_f is the total fission cross section of the region

This particularity of the Samarium-149 depletion is obvious in the curve 3.14. Therefore, the error on the computation of the Samarium-149 density is not increased when total power is modified.

Plutonium-239 is also an important isotope. It is a significant source of energy during the operation of a reactor. The concentration of this isotope does not seem to be affected by local effects due to the modification of the global power of the assembly.

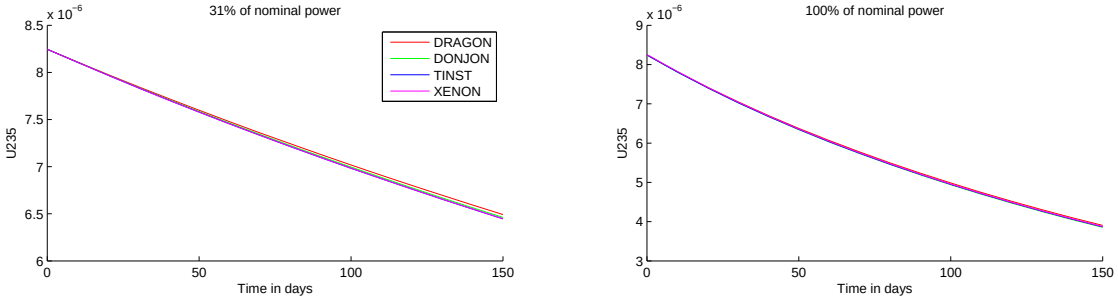

Figure 3.11 Benchmark 2 : Uranium-235 density for the two calculations

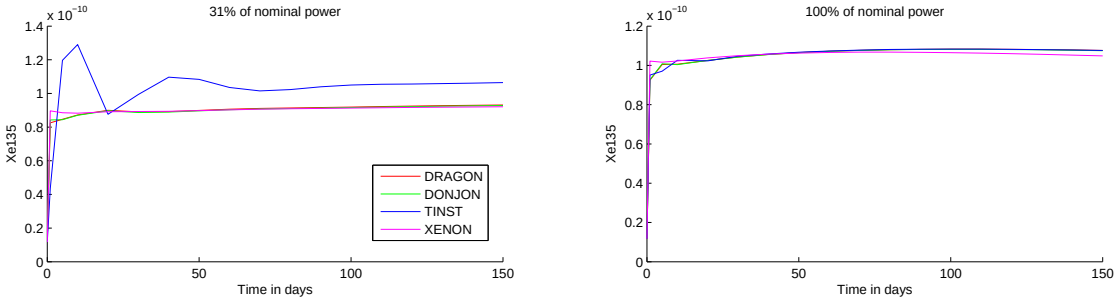

Figure 3.12 Benchmark 2 : Xenon-135 density for the two calculations

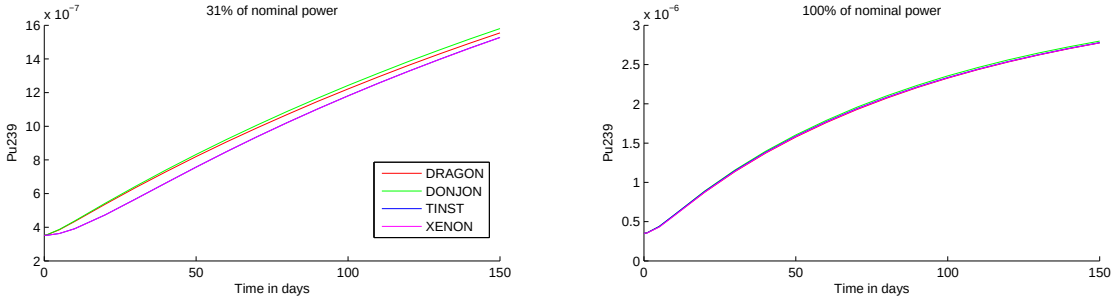

Figure 3.13 Benchmark 2 : Plutonium-239 density for the two calculations

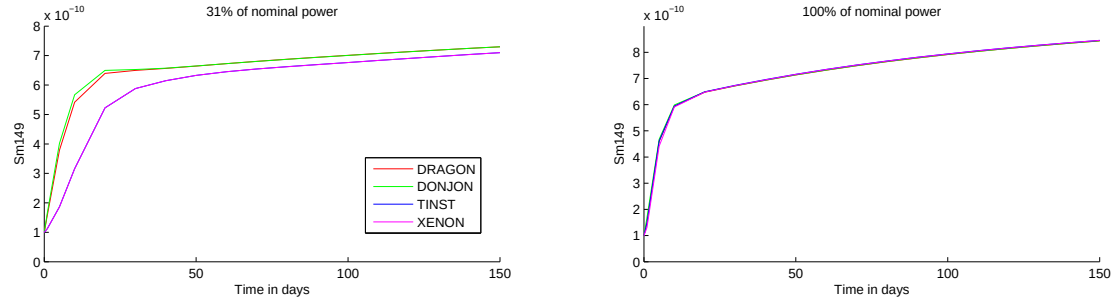

Figure 3.14 Benchmark 2 : Samarium-149 density for the two calculations

Tables 3.8, 3.7, and 3.9 give the final relative differences of Uranium-235, Xenon-135 and Plutonium-239 according to the different methods. The numerical results are given as a percentage, and represents the deviation to the DRAGON reference case.

Table 3.7 Benchmark 2: Relative differences (in %) of Xenon-135 density after 150 days

Method	P_{nom}	$0.31 \times P_{nom}$
DONJON	-0.14	-0.32
TINST	-0.05	12.50
XENON	-2.68	-1.12

Table 3.8 Benchmark 2: Relative differences (in %) of Uranium-235 density after 150 days

Method	P_{nom}	$0.31 \times P_{nom}$
DONJON	-1.21	-0.47
TINST	-0.90	-0.70
XENON	-0.73	-0.69

Table 3.9 Benchmark 2: Relative differences (in %) of Plutonium-239 density after 150 days

Method	P_{nom}	$0.31 \times P_{nom}$
DONJON	0.81	1.60
TINST	0.11	-1.77
XENON	0.02	-1.82

As previously observed, results are very concordant concerning Uranium-235. The error is under 1.2% regardless of the method used. Even for this isotope, the error seems to be reduced with micro-depletion method at low power. For Xenon-135, the evaluation of the interpolated concentration is inaccurate at low power. There is an error of 12.50 %. This error is reduced to 0.32 % when micro-depletion is used, and to 1.12 % when the `XENON:` module is used. For Plutonium-239, the deviations are less important than for Xenon. The micro-depletion appears to be less accurate than interpolation for the nominal power calculation. All the methods seem to be equivalent at low power.

Final Xenon distributions are illustrated in Figures 3.15 and 3.16. It is interesting to notice the particular shape of the distribution.

For $P = P_{nom}$, the average value of Xenon-135 concentration is the same if we use a micro-depletion method or an interpolation method. It corresponds to the saturated concentration at nominal power. A difference appears in the right lower-corner. The depression is stronger in the case of micro-depletion. As the neutronic flux is lower in this part of the geometry, the saturated concentration is decreased. The value of the interpolated Xenon concentration in right lower-corner is less consistent with the value of the flux.

For $P = 0.31 \times P_{nom}$, we see also clearly the depression in the distribution. Also, one notices that the average value of the concentration is lower in micro-depletion. It is more consistent than using interpolation because the global power of the assembly is reduced. Bundles operating at low powers have a Xenon concentration lower to the other bundles. This phenomenon is more significant in the case of micro-depletion.

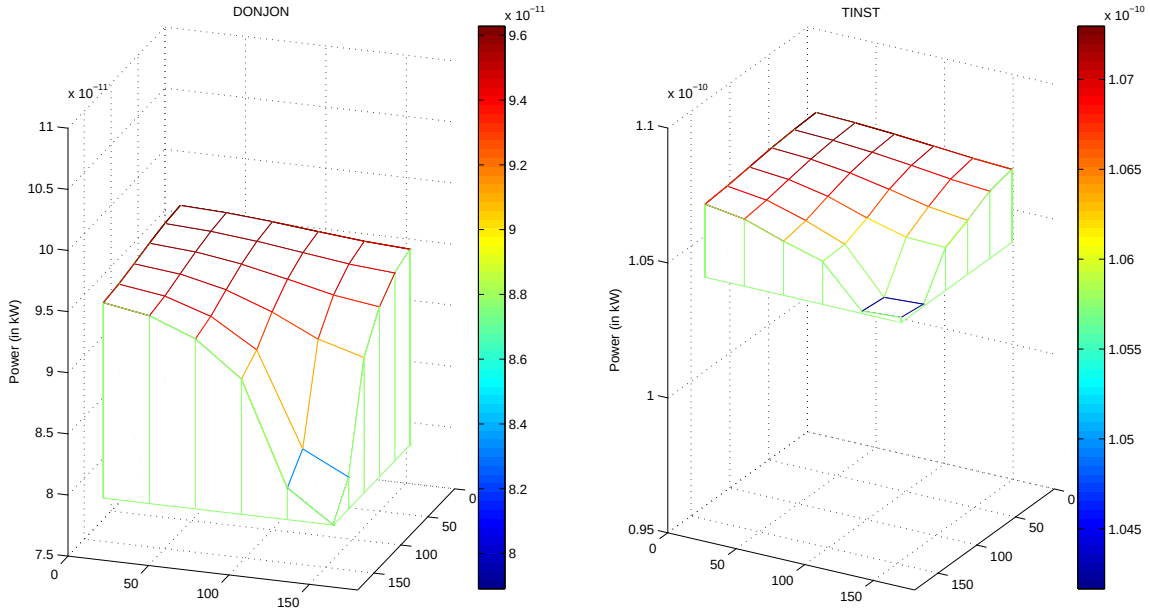

Figure 3.15 Benchmark 2: Xenon distribution for $P = 10.0\ kW/kg$

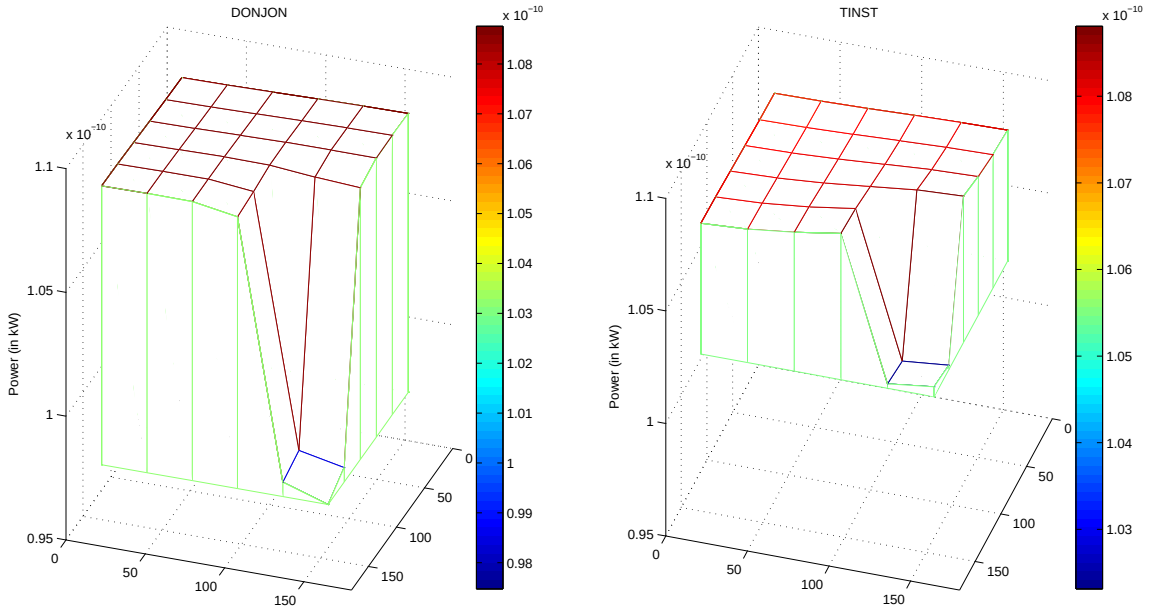

Figure 3.16 Benchmark 2: Xenon distribution for $P = 31.97\ kW/kg$

3.3.3 Conclusions

The study of the previous simulations allows to reach the following conclusions :

- For nominal conditions, the `TINST` method is closer to the DRAGON results. The addition of the Xenon correction is not useful in this case. On the contrary, it tends to bias the multiplication factor. The calculation of isotopic concentrations is accurate regardless of the method used. Even if the flux is not the nominal flux in each bundle, the computation of Xenon concentration is relatively accurate at this power. Only four bundles on thirty six are operating at a power lower to nominal conditions. Therefore, the contribution of low power bundles is not a large source of error in this case.
- For low power depletion, the interpolation method gives bad results. A part of the error can be attributed to the Xenon evaluation. The correction with the `XENON:` module provides a net improvement on the multiplication factor. It provides a gain of 4 mk. However, a gap remains between the `XENON` simulation and DRAGON. This can be due to other isotopes that have a particular behavior with local powers.

CHAPTER 4

CANDU-6 CORE FOLLOW-UP

4.1 Reactor model

2-group properties are generated using the DRAGON transport code for the fuel, the reflector and the devices. In CANDU reactors, fuel channels cross reactivity mechanisms such as adjusters and liquid zone controllers at a right angle. Appropriate 3D supercell models are thus required to generate consistent properties for these devices. The CANDU-6 reactor is composed of [16] :

- 380 channels of 12 fuel bundles
- A reflector zone which surrounds the fuel zone. The width of the reflector zone can vary from one plane to another.
- Adjuster rods and guide tubes
- Liquid zone controllers and guide tubes
- Mechanical absorber, shutdown system rods, detector, SDS2 poison injector guide tubes
- Adjuster supporting bars and cables
- Device brackets and locators
- Device tensioning springs and coupling nuts

A CANDU-6 core follow-up is a set of calculation schemes executed one after the other. At each step, a set of parameters is modified. Usually, the following quantities are changed:

- Moderator purity
- Poison load (Boron)
- Insertion rate of each liquid zone controller
- A set of channels to refuel according to a bidirectional refueling scheme
- Fuel depletion time

Properties for devices are assumed to be independent of the moderator poison load and fuel burnups. After a calculation, the burnup and the power distributions are computed over the reactor and transferred to the next calculation point. In the case of a micro-depletion, we have also to transmit the microscopic cross sections library.

4.2 Presentation of the simulations

4.2.1 Introduction

The Gentilly-2 reactor operating history from 3200.8 to 3256.2 Full Power Days (FPD) was simulated using the chain of codes DRAGON/DONJON. This operating history is represented by around 30 simulation time steps. Core-follow simulations had been already performed using DONJON3 [17] [18].

The core follow-up is performed according to the two methods previously introduced. For the macroscopic depletion method, two different calculations are done: with the use of the `XENON:` module and without. The goal is to underline the influence of the `XENON:` module on a CANDU-6 reactor simulation. Two microscopic depletion computations are compared. The first case uses a single depletion chain for each fuel cell. This depletion chain results from a total homogenization of the CANDU-6 fuel cell at lattice level. Two independent depletion chains are computed for the second microscopic depletion computation. These two different depletion chain are produced during the homogenization process at lattice level, as described in Chapter 1. The scheme 4.1 depicts the process used for our second micro-depletion core-follow simulation.

Equation 1.25 gives the way microscopic cross sections are computed. They are homogenized and condensed by regions. Here, we choose to homogenize the rows of fuel pins differently for our second micro-depletion calculation. The peripheral row of pins gives birth to a second depletion chain. The rest of the fuel pins are homogenized together in another depletion chain. Moderator properties and contribution of non-extracted isotopes are included in the residual isotope.

When multiplied by the cell flux, homogenized microscopic cross sections of the peripheral row of fuel pins produces peripheral fuel pins reaction rates. No form factors are required to correct the bundle flux. Here, the rows of fuel pins are homogenized separately in the `EDI:` module of DRAGON. This capability of the chain of codes DRAGON/DONJON has been developed for the need of this project.

Figure 4.1 Two types of homogenization for the micro-depletion core follow-up

4.2.2 The sequential call to DONJON modules

DONJON calculations are based on the TRIVAC multigroup diffusion solver. The resolution method is a mesh-centered finite difference. Fluxes are obtained at a precision of 10^{-6}. In a core follow-up, a sequential call to modules is done for each input file. The modular call differs slightly if we use a micro-depletion method. The two next subsections give a description of the modules used for the two different calculations.

4.2.3 The sequential call to DONJON modules for the interpolation method

- Geometry construction and tracking
- Devices definition
- Detectors definition
- Fuel map object construction, including burnups and powers over the fuel geometry
- Refueling scheme and depletion
- Setting of liquid zone controllers level
- Setting of moderator purity and boron load
- Interpolation of devices and reflectors properties
- Construction of the complete library, including fuel properties
- Diffusion solving : computation of fluxes and powers over the reactor

4.2.4 The sequential call to DONJON modules for the micro-depletion method

- Geometry construction and tracking
- Devices definition
- Detectors definition
- Fuel map object construction, including burnups and powers over the fuel geometry

- Fuel map geometry construction and tracking
- Refueling scheme and depletion to compute the residual properties
- Setting of liquid zone controllers level
- Setting of moderator purity and boron load
- Interpolation of devices and reflectors properties
- Construction of the complete library, including fuel properties
- Refueling performed on the microscopic cross section library
- New interpolation to update the residual properties
- Diffusion solving : computation of fluxes and powers over the reactor

4.2.5 Example of input files

The input files used in this project are transferred from the equivalent DONJON3 core follow-up [16] [19]. Two Fortran transfer programs are required to transfer the CLE-2000 files. To run the core follow-up, an execution script is written. An example of input file and execution script is given in Appendix B.

4.3 Results

Four follow-ups are run. Two of them are micro-depletion follow-ups, and the two others are based on an interpolation method. A brief description of each simulation is given below. The acronyms are concordant with the one used for the result analysis (tables, curves).

`EVO 1`	Micro-depletion method with one depletion chain within a fuel cell.
`EVO 2`	Micro-depletion method with two different depletion chains within a fuel cell.
`TINST`	Interpolation method without correction of the Xenon distribution.
`XENON`	Interpolation method with the use of the `XENON:` module.

4.3.1 Effective multiplication factor

The effective multiplication factor is computed at each time step according to the different methods. When simulations of reactor normal operation are performed, the core multiplication factor is not an indicator of the accuracy of the results. Comparison with local values are generally preferred, such as bundle powers.

The daily loss of reactivity as fuel depletes is compensated for by on-line refueling. That explains the irregular shape of the curves. The modification of the Boron density in the core is also performed to change the criticality of the core. The k_{eff} remains between 1.007 and 0.999 regardless of the method used.

During the first days of depletion, we observe a noticeable increase of the k_{eff} in micro-depletion calculation. This can be explained by the fact that initial densities are interpolated densities. Basically, Xenon concentrations correspond to saturated concentrations. A readjustment of isotopic densities to the local flux has thus to be achieved in each bundle. During the first days, the depletion solver recomputes the Xenon concentrations. Therefore, the k_{eff} increases at the beginning of the follow-up. After that, the evolution is very consistent with the `TINST` follow-up. The curves have the same shape. The maximum discrepancy is 1.81 mk at 3209.6 FPD.

The correction of the Xenon-135 concentrations does not have a large influence on the reactivity of the reactor. During the entire simulation, the multiplication factor of the `XENON` follow-up overestimates the multiplication factor of the `TINST` follow-up by less than 1 mk. As noticed before, the additional calculation time required for this method is negligible.

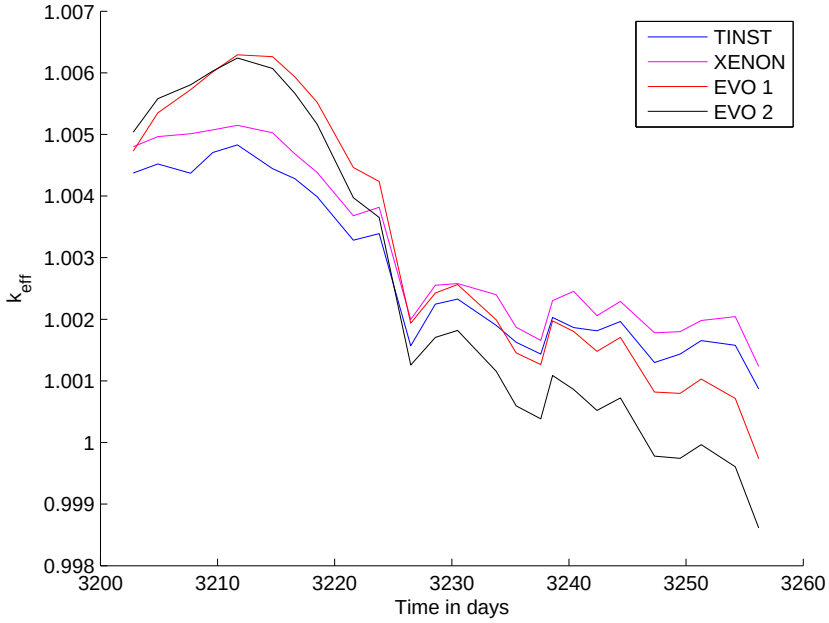

Figure 4.2 Core Follow: Effective multiplication factor

The use of a micro-depletion method has a small impact on the reactivity evaluation. The separate depletion of fuel rings has also a limited effect. This is conceivable, as the improvements due to the method are supposed to be rather local than global.

In the previous chapter, we observed that the evaluation of the k_{eff} was inaccurate with an interpolation method, when the bundle power was low. During the operation of the reactor, local powers change according to the fuel burnups and the channel refueling. Some bundles deplete at low powers, whereas others are exposed to high powers.

To link up our present results with the Benchmark studies, we have to take a look at the power distribution while the core is operating. Even if local burnups change at each time step, the global distribution remains almost unchanged. The following bar graph gives a representation of the distribution of bundle powers.

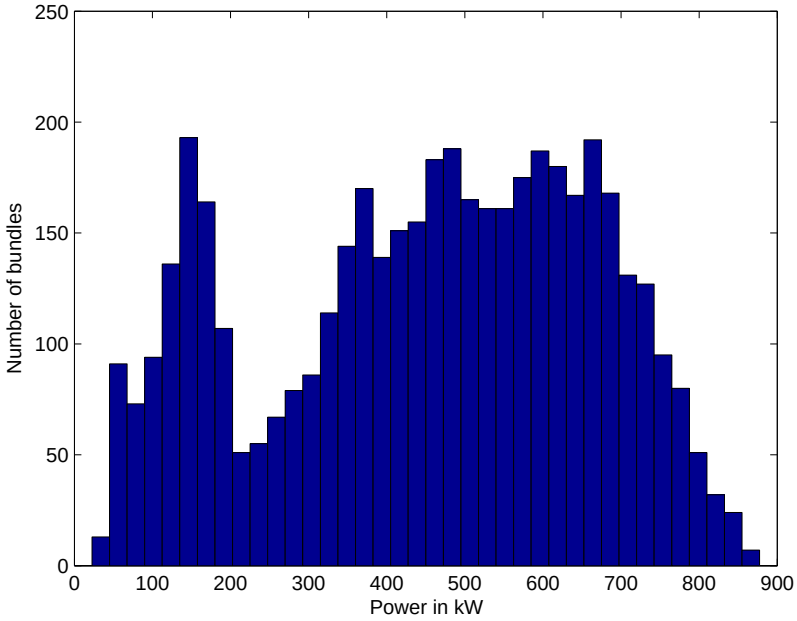

Figure 4.3 Bundle power distribution at 3256.2 FPD

This distribution is condensed in four power groups: lower to 10% of the nominal power (about 615 kW), between 10 and 50%, between 50 and 100%, and higher to 100%. It is plotted in Figure 4.4. The values are also written in the Table 4.1.

Table 4.1 Distribution of bundle powers

	$\leq 10\%$	$10-50\%$	$50-100\%$	$\geq 100\%$
Number of bundles	91	1132	2288	1049
Percentage of bundles	1.99%	24.8%	50.2%	23.0%

The layout of the power distribution reveals two different zones. The largest zone is between 400 and 700 kW. Another peak is present at low power. Basically, it corresponds to the peripheral bundles of the reactor. As described in Chapter 3, the multiplication factor of these bundles tends to be biased by the `TINST` method. However, this phenomenon does not seem to affect the multiplication factor of the reactor. The large number of bundles operating at high powers reduces the discrepancy between the two methods.

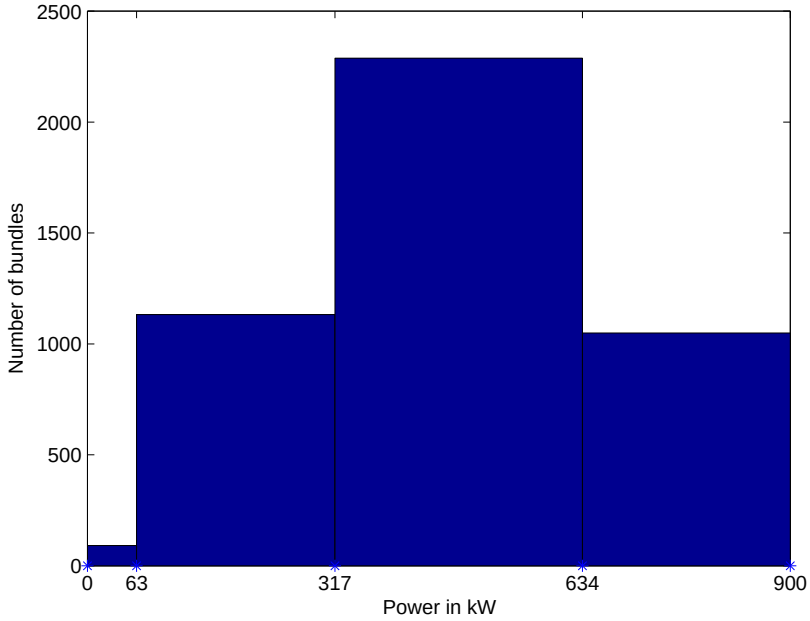

Figure 4.4 Condensed bundle power distribution at 3256.2 FPD

4.3.2 Micro-depletion follow-ups

Results coming from the two micro-depletion follow-ups are compared in this section. The goal is to evaluate the gain provided by the separate depletion of the fuel rings. Table 4.2 presents the concentration relative difference between `EVO 1` and `EVO 2` for some important nuclides. It corresponds to the results obtained at the end of the simulation.

The concentration bias computed in the table are the maximum bias occurring in the reactor. Obtaining larger errors for nuclides with low densities (such as Pu240, Pu241, Pm148 or Pm148m) is expected as these nuclides are at the end of the isotopic chains. Except for theses isotopes, the maximum bias is below 3 % between the two calculations. We can point out that the relative discrepancies are lower for the initial isotopes (U235, U238) in comparison to the subsequent isotopes (other actinides and fission products).

For Samarium-149 and Xenon-135, the bias is very low (less than 1%). So the handling of local effects does not seem to be improved by the consideration of the different fuel rings.

Table 4.2 Concentration bias between the two micro-depletion simulations

Isotope	Error (in %)
U238	0.002
U235	0.56
Pu239	2.30
Pu240	5.58
Pu241	9.11
Np239	2.31
Xe135	0.79
Sm149	1.74
Pm147	2.30
Pm148	4.02
Pm148m	3.88

Performing the second microscopic depletion calculation takes twice the time needed for the first. The computing time needed for one calculation point is about 10 hours for the `EVO 2` follow-up. Therefore, one notices that the improvement provided by the separation of depletion calculations for the fuel is not worthwhile, given the additional computational time required.

4.3.3 Power distribution

To understand how the local effects are handled by the different methods, a study of the power distribution is performed. First, the channel powers are laid out. Then, a study of the axial power distribution of the reactor is conducted to underline the phenomenon.

Channel powers

Channel powers distribution in micro-depletion is compared with the interpolation calculation, with and without the use of the `XENON:` module. The comparison is performed at the final point of calculation, which is 3256.2 FPD. At the beginning of our follow-up, the powers are the same regardless of the method used, because they are imposed by the first interpolation. The relative differences are shown in Figures 4.5 and 4.6. The estimation of the gap between the different cases is made with the formulas 4.1 and 4.2 :

$$\epsilon_1^{chan} = 1000 \cdot \frac{P_{\texttt{TINST}}^{chan} - P_{\texttt{EVO}}^{chan}}{P_{\texttt{TINST}}^{chan}} \tag{4.1}$$

$$\epsilon_2^{chan} = 1000 \cdot \frac{P_{\texttt{XENON}}^{chan} - P_{\texttt{EVO}}^{chan}}{P_{\texttt{XENON}}^{chan}} \tag{4.2}$$

On average, the relative differences are equal to 2.2% for the `TINST` and 4% for the `XENON` methods. For certain channels, the discrepancy can reach 10 %. It occurs once for the `TINST` simulation and five times for the `XENON` simulation. Globally, the channel powers are not too much affected by the method of resolution. Given that the total power of the core is imposed, an error on a channel has an impact everywhere in another channel. In the previous studies, we observed that the Xenon correction is pertinent for bundles depleting at low powers, but it could bias slightly the results otherwise. Because of the frequent refueling, the Xenon-135 concentration is not the balance concentration everywhere in the reactor.

	01	02	03	04	05	06	07	08	09	10	11	12	13	14	15	16	17	18	19	20	21	22	
A									11	-11	9	12	1	-15									A
B						-26	16	22	-10	-12	15	- 8	22	-36	- 0	-10	-18						B
C					-15	21	31	22	20	8	- 5	-11	39	-15	-26	5	15	-13					C
D				30	22	-18	3	27	- 9	-83	- 2	- 5	39	-34	14	19	-11	15	0				D
E			51	34	9	-32	-24	-21	-11	- 8	24	5	10	- 5	-19	-23	5	37	32	10			E
F			39	48	35	21	22	- 5	-37	11	- 8	20	13	15	- 4	2	5	32	12	12			F
G		61	37	53	14	-16	-25	-31	2	- 3	23	11	23	26	35	- 2	-32	16	45	25	56		G
H		46	51	29	-14	-10	- 3	2	13	20	25	-27	11	27	- 3	6	25	27	-36	12	59		H
J	22	51	50	16	7	-25	-43	-30	10	3	1	-22	23	30	42	-20	-16	- 1	-16	31	26	18	J
K	58	24	43	-21	- 3	10	- 1	- 4	-13	21	30	-14	9	15	-34	- 8	3	-29	24	- 8	15	50	K
L	44	47	50	12	- 4	- 6	-43	15	18	21	34	23	18	31	10	-43	-23	-50	-12	39	37	48	L
M	-46	17	40	- 7	-34	1	-12	29	26	6	6	38	32	20	- 5	-19	- 0	-16	-13	- 9	14	45	M
N	33	24	-39	-23	-44	-34	-10	-27	15	1	26	-30	9	-19	-20	-54	-41	-21	-22	9	39	30	N
O	29	38	39	12	- 1	-49	-19	38	24	25	14	14	5	20	3	-16	-28	-33	13	39	11	41	O
P		55	38	6	-17	- 2	-15	-13	1	- 7	10	-35	17	-11	12	-52	-20	-39	11	13	47		P
Q		53	-35	-29	-21	- 3	-99	-35	-19	15	24	6	30	30	-21	-35	- 7	-10	- 3	1	39		Q
R			7	29	- 1	-26	- 5	30	9	-10	22	22	27	13	2	- 9	-47	-34	-29	38			R
S			4	-11	11	- 8	-10	13	34	14	4	18	22	31	- 1	-35	- 5	14	4	-13			S
T				-20	7	- 5	- 4	- 4	-25	34	4	- 9	2	- 9	- 1	6	8	4	30				T
U					-34	-26	-30	-51	-61	-50	-61	-36	8	-16	-31	-62	-47	-13					U
V						-59	-25	-34	-34	-29	-62	-22	37	-52	-26	-48	-57						V
W									-63	-33	-27	-28	27	-19									W
	01	02	03	04	05	06	07	08	09	10	11	12	13	14	15	16	17	18	19	20	21	22	

Figure 4.5 Relative Differences ϵ_1^{chan} for channel powers at 3256.2 FPD (in % *10)

	01	02	03	04	05	06	07	08	09	10	11	12	13	14	15	16	17	18	19	20	21	22	
A									41	41	22	44	34	20									A
B						3	11	6	21	20	19	44	16	3	30	39	8						B
C					12	0	57	47	9	38	40	-26	3	25	52	30	40	12					C
D				61	46	38	17	47	-35	51	32	32	0	5	36	38	7	33	27				D
E			86	61	23	43	-35	8	10	20	5	43	53	37	0	-10	4	50	53	42			E
F			74	74	47	23	21	8	21	12	36	14	52	55	- 7	4	5	38	31	40			F
G		99	69	69	15	- 6	-35	-31	17	26	6	46	60	62	27	- 8	-44	12	52	50	93		G
H		86	82	42	-21	- 7	-18	- 9	6	33	47	55	20	60	- 1	-25	-45	-38	-38	35	96		H
J	64	88	70	12	-28	-57	-72	-42	17	18	21	48	3	60	43	-42	-48	-28	- 3	38	51	55	J
K	99	61	60	-28	-25	-50	-37	-25	-13	13	47	36	13	42	-45	-38	-38	-62	-42	-13	43	92	K
L	90	83	65	- 1	-37	-53	-86	-41	15	26	48	39	41	57	5	-78	-71	-90	-12	40	64	91	L
M	-90	47	52	-21	-69	-54	-62	-58	30	11	18	56	53	44	-10	-59	-52	-62	-39	- 9	35	3	M
N	76	57	-51	- 7	-85	-89	-59	-55	21	2	38	46	6	1	-36	-94	-96	-71	-52	10	62	70	N
O	9	65	48	- 7	-41	-99	-70	-67	18	30	27	26	23	40	13	-56	-83	-81	-19	-35	29	77	O
P		87	56	- 2	-15	-51	-68	-49	14	- 2	4	-50	2	3	-39	-99	-73	-81	-11	-20	74		P
Q		80	51	-20	-52	-50	-99	-70	-37	19	32	21	49	48	-47	-79	-57	-50	-24	2	61		Q
R			21	31	-22	-64	-51	-70	-12	- 3	26	29	42	30	-29	-55	-90	-64	-19	50			R
S			16	-13	-10	-28	-52	-48	53	5	3	25	35	47	-25	-75	-45	-15	-16	-20			S
T				-23	- 6	-22	-33	-31	-49	-51	4	9	3	0	-31	-43	-41	-17	-34				T
U					-40	-47	-61	-87	-93	-78	-80	-44	9	-13	-63	-97	-75	-26					U
V						-75	-50	-65	-64	-56	-86	-38	48	-58	-57	-77	-77						V
W									-89	-62	-57	-58	56	-50									W
	01	02	03	04	05	06	07	08	09	10	11	12	13	14	15	16	17	18	19	20	21	22	

Figure 4.6 Relative Differences ϵ_2^{chan} for channel powers at 3256.2 FPD (in % *10)

Axial powers

The power deviations to the micro-depletion follow-up (in MW) are summed up in table 4.3 for each plane.

Table 4.3 Power deviations according to the axial position in the reactor (in MW)

Method	TINST	XENON	Total power
Plane 1	-8.81	-8.33	46.90
Plane 2	-15.00	-15.72	118.16
Plane 3	-10.12	-12.78	168.10
Plane 4	0.648	-3.26	198.93
Plane 5	12.57	8.81	233.81
Plane 6	21.62	18.96	252.31
Plane 7	21.76	20.86	253.04
Plane 8	12.91	13.78	236.05
Plane 9	0.550	3.01	203.17
Plane 10	-10.71	-6.58	175.41
Plane 11	-16.05	-11.73	125.36
Plane 12	-9.38	-7.05	50.00

For the TINST calculation, the power is inferior to the micro-depletion in the planes 1, 2, 3, 10, 11 and 12. Theses planes are located at the extremity of the core. Hence, they are exposed to low powers. So, the deviation can be explained by the overestimation of the Xenon 135 concentration. As the balance density of Xenon 135 is higher in these regions than in micro-depletion, the neutronic flux is reduced, and therefore the power too. To compensate this phenomenon, the power is higher in the intermediate planes.

We observe that the deviations are slightly reduced with the Xenon correction. The absolute deviation is 131 MW against 141 MW without the XENON: module. Hence, Xenon-135 is not the only responsible of the deviations in peripheral planes. Others power-dependent isotopes are not well estimated in these zones.

A study of the power distribution in the first plane is done in the following. As for the channel powers, the comparison is done at 3256.2 FPD. The relative differences in the first plane of the core are shown in Figures 4.7 and 4.8. The estimation of the deviation between the different follow-ups is made with the formulas 4.3 and 4.4.

$$\epsilon_1^{plane} = 100 \cdot \frac{P_{\texttt{TINST}}^{plane} - P_{\texttt{EVO}}^{plane}}{P_{\texttt{TINST}}^{plane}} \tag{4.3}$$

$$\epsilon_2^{plane} = 100 \cdot \frac{P_{\texttt{XENON}}^{plane} - P_{\texttt{EVO}}^{plane}}{P_{\texttt{XENON}}^{plane}} \tag{4.4}$$

The relative differences are higher than for the channel powers. The bundles in the first plane are more prone to the influence of the local power effect. The flux is reduced in this part of the reactor. The Xenon-135 correction helps to decrease the error. For instance, 27.5% of the bundles have a relative deviation superior to 25% with the `XENON:` module, while 46.1% without.

	01	02	03	04	05	06	07	08	09	10	11	12	13	14	15	16	17	18	19	20	21	22	
A									-23	-25	-24	-26	25	-27									A
B						-25	-22	-26	-24	-26	-27	-30	29	-31	-26	-26	-24						B
C					-22	-25	-23	-22	-25	-30	-30	-32	30	-30	-25	-26	-25	-24					C
D				-21	-22	-22	-23	-23	-28	-45	-31	-30	27	-28	-27	-26	-24	-23	-22				D
E			-19	-19	-22	-22	-23	-27	-29	-31	-29	-28	25	-25	-30	-24	-23	-22	-21	-20			E
F			-21	-20	-21	-22	-23	-25	-27	-26	-28	-25	26	-23	-24	-21	-21	-19	-17	-21			F
G		-19	-21	-19	-22	-23	-24	-24	-26	-25	-25	-23	25	-22	-24	-18	-26	-20	-17	-17	-18		G
H		-18	-18	-17	-23	-20	-20	-21	-23	-26	-23	-24	22	-24	-25	-23	-22	-21	-20	-18	-20		H
J	-19	-18	-17	-19	-18	-19	-24	-25	-23	-26	-24	-25	27	-25	-24	-24	-23	-22	-20	-20	-19	-20	J
K	-19	-21	-19	-19	-20	-22	-21	-24	-27	-27	-25	-23	26	-25	-26	-20	-18	-21	-21	-17	-22	-18	K
L	-18	-17	-16	-17	-19	-19	-20	-23	-23	-26	-23	-26	25	-26	-25	-23	-23	-21	-20	-19	-20	-20	L
M	-20	-19	-18	-19	-20	-21	-24	-28	-27	-25	-28	-24	27	-26	-25	-24	-19	-19	-19	-17	-19	-22	M
N	-21	-18	-14	-18	-24	-19	-22	-26	-27	-28	-25	-27	29	-29	-28	-26	-24	-22	-22	-18	-19	-22	N
O	-36	-20	-19	-21	-20	-21	-25	-28	-29	-26	-30	-26	29	-27	-27	-25	-20	-21	-17	-17	-21	-21	O
P		-21	-21	-19	-19	-20	-22	-25	-28	-27	-28	-27	28	-29	-26	-25	-19	-22	-19	-18	-19		P
Q		-19	-19	-19	-18	-18	-26	-26	-29	-30	-26	-29	27	-28	-29	-26	-21	-21	-22	-20	-22		Q
R			-21	-19	-19	-23	-20	-22	-25	-28	-30	-28	26	-28	-26	-24	-21	-20	-21	-21			R
S			-20	-22	-22	-23	-25	-25	-27	-26	-29	-26	27	-26	-25	-22	-21	-20	-21	-19			S
T				-21	-22	-23	-24	-26	-30	-27	-29	-26	29	-25	-25	-23	-21	-20	-20				T
U					-22	-25	-25	-26	-29	-32	-30	-28	29	-27	-27	-29	-26	-22					U
V						-25	-26	-29	-31	-28	-30	-29	30	-31	-27	-25	-24						V
W									-27	-27	-29	-28	29	-23									W
	01	02	03	04	05	06	07	08	09	10	11	12	13	14	15	16	17	18	19	20	21	22	

Figure 4.7 Relative Differences ϵ_1^{plane} for the first plane at 3256.2 FPD (in %)

	01	02	03	04	05	06	07	08	09	10	11	12	13	14	15	16	17	18	19	20	21	22	
A									-16	-19	-17	-19	19	-20									A
B						-18	-16	-21	-19	-21	-21	-24	22	-23	-21	-19	-17						B
C					-15	-19	-18	-18	-20	-25	-25	-26	24	-23	-21	-21	-19	-18					C
D				-14	-16	-18	-19	-20	-25	-41	-26	-25	21	-21	-24	-22	-19	-17	-16				D
E			-12	-13	-17	-19	-21	-25	-26	-26	-24	-22	19	-18	-27	-22	-21	-18	-16	-14			E
F			-14	-14	-17	-20	-22	-24	-25	-23	-24	-20	21	-17	-23	-21	-20	-16	-13	-15			F
G		-12	-15	-15	-20	-22	-24	-24	-24	-22	-22	-19	19	-17	-24	-20	-26	-18	-14	-13	-11		G
H		-11	-13	-14	-22	-21	-21	-22	-22	-24	-20	-20	18	-19	-25	-24	-23	-21	-18	-15	-13		H
J	-12	-13	-14	-17	-19	-20	-26	-25	-22	-24	-20	-21	21	-19	-24	-25	-24	-22	-20	-18	-15	-13	J
K	-12	-16	-17	-18	-21	-23	-23	-25	-26	-26	-22	-20	21	-19	-26	-22	-21	-23	-21	-15	-18	-12	K
L	-11	-13	-13	-17	-21	-22	-23	-24	-23	-25	-21	-21	20	-21	-25	-25	-25	-23	-21	-17	-17	-14	L
M	-14	-15	-17	-19	-22	-24	-26	-29	-26	-23	-25	-21	22	-20	-26	-26	-22	-22	-20	-16	-16	-17	M
N	-15	-14	-14	-18	-26	-22	-25	-28	-26	-26	-22	-23	23	-23	-29	-28	-27	-24	-23	-18	-17	-17	N
O	-29	-16	-18	-21	-22	-24	-28	-29	-28	-24	-26	-22	24	-21	-28	-27	-23	-23	-18	-17	-19	-15	O
P		-16	-18	-18	-20	-22	-25	-27	-28	-26	-26	-23	24	-23	-27	-28	-21	-24	-19	-16	-15		P
Q		-14	-16	-18	-19	-20	-28	-27	-28	-29	-24	-25	22	-22	-29	-27	-24	-23	-21	-18	-17		Q
R			-16	-17	-19	-24	-22	-23	-25	-27	-28	-26	22	-23	-26	-26	-23	-21	-19	-17			R
S			-16	-19	-21	-23	-26	-26	-26	-25	-27	-23	23	-21	-25	-23	-22	-20	-19	-16			S
T				-18	-20	-22	-25	-26	-29	-26	-27	-23	25	-21	-26	-23	-21	-19	-17				T
U					-19	-23	-24	-27	-28	-30	-28	-26	25	-23	-27	-29	-24	-20					U
V						-22	-24	-27	-29	-27	-29	-27	27	-26	-26	-24	-22						V
W									-24	-25	-27	-26	27	-24									W
	01	02	03	04	05	06	07	08	09	10	11	12	13	14	15	16	17	18	19	20	21	22	

Figure 4.8 Relative Differences ϵ_2^{plane} for the first plane at 3256.2 FPD (in %)

4.3.4 Study of the Xenon distribution

As for the powers, the Xenon distribution is showed in two configurations. The first corresponds to the densities per channel. The second study provides the density map in the first plane of the reactor. In the periphery of the core, the Xenon effect is supposed to be the most important. The concentrations are computed in reference to the `EVO 1` case.

For the two configurations, the deviations are computed according to formulas 4.5, 4.6, 4.7 and 4.8. Bundles are colored according to the value of the deviation : yellow (between 10 and 20 %), orange (between 20 and 30 %), red (between 50 and 100 %) and black (more than 100 %).

$$\epsilon_1^{chan} = 100 \cdot \frac{N_{X_{\texttt{TINST}}}^{chan} - N_{X_{\texttt{EVO}}}^{chan}}{N_{X_{\texttt{TINST}}}^{chan}} \tag{4.5}$$

$$\epsilon_2^{chan} = 100 \cdot \frac{N_{X_{\texttt{XENON}}}^{chan} - N_{X_{\texttt{EVO}}}^{chan}}{N_{X_{\texttt{XENON}}}^{chan}} \tag{4.6}$$

$$\epsilon_1^{plane} = 100 \cdot \frac{N_{X_{\texttt{TINST}}}^{plane} - N_{X_{\texttt{EVO}}}^{plane}}{N_{X_{\texttt{TINST}}}^{plane}} \tag{4.7}$$

$$\epsilon_2^{plane} = 100 \cdot \frac{N_{X_{\texttt{XENON}}}^{plane} - N_{X_{\texttt{EVO}}}^{plane}}{N_{X_{\texttt{XENON}}}^{plane}} \tag{4.8}$$

The evaluation of Xenon concentrations seems to be more biased at the border of the reactor. Some peripheral channels show a discrepancy of 10 % in comparison to micro-depletion. The correction using the `XENON:` module is very efficient. It reduces the largest deviations. All the relative differences are within 8 %.

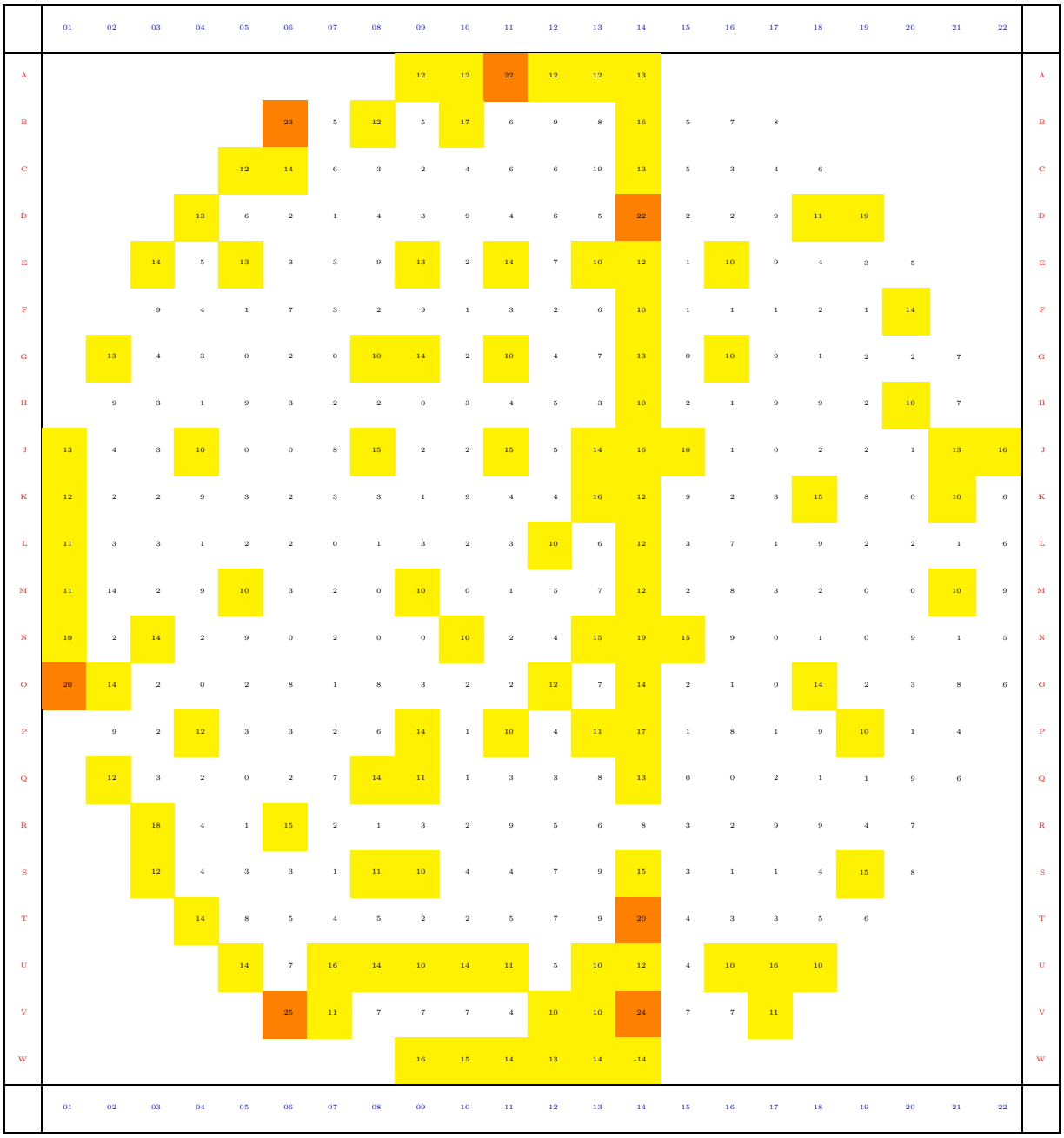

Figure 4.9 Relative differences ϵ_1^{chan} of Xenon-135 densities per channel at 3256.2 FPD (in %)

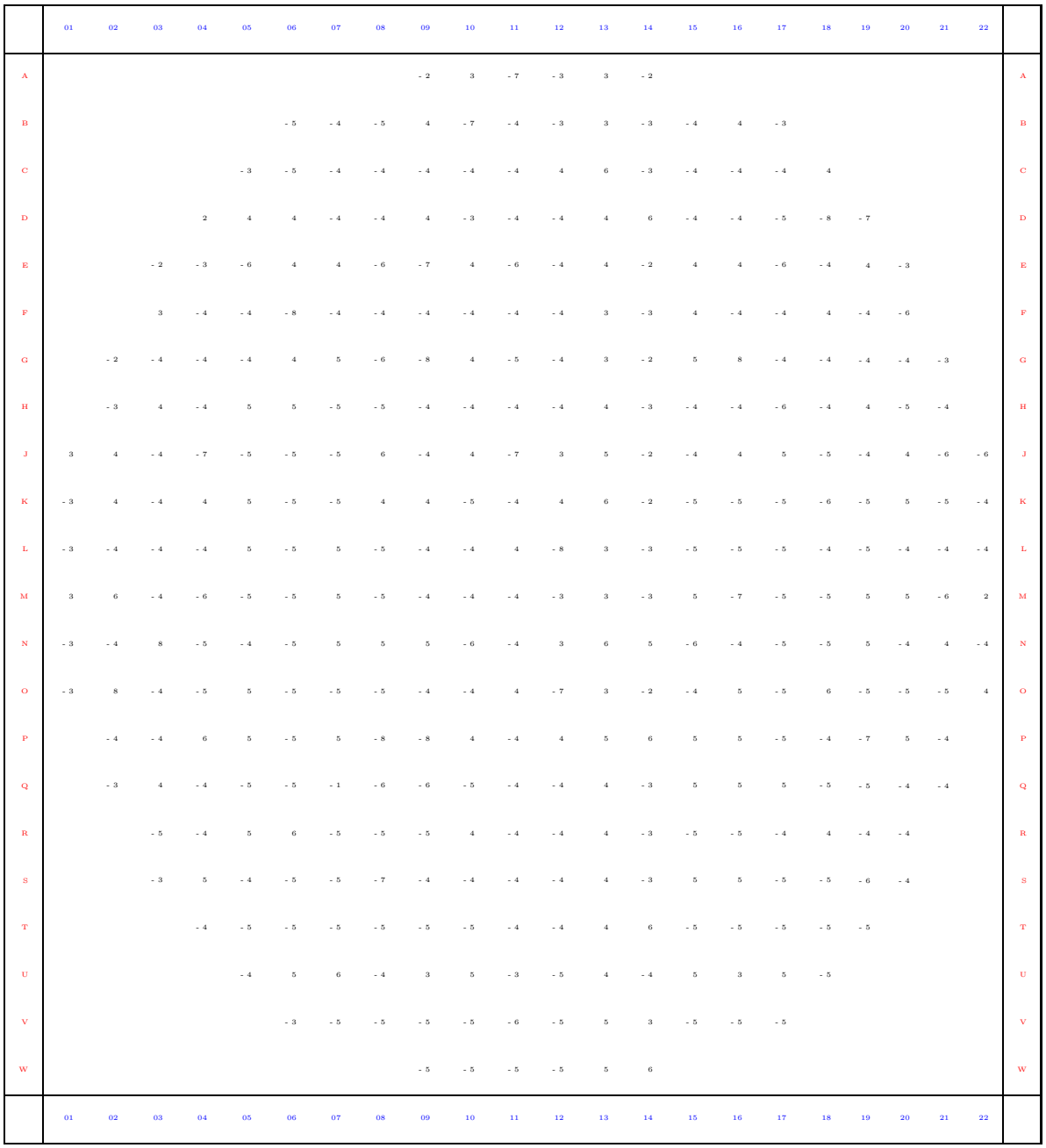

Figure 4.10 Relative differences ϵ_2^{chan} of Xenon-135 densities per channel at 3256.2 FPD (in %)

Axial Xenon distribution

The density deviations (in %) are summed up in the table 4.4 for each plane.

Table 4.4 Xenon average deviations according to the axial position in the reactor (in %)

Method	TINST	XENON
Plane 1	24.67	-6.99
Plane 2	7.41	-3.74
Plane 3	3.32	-2.46
Plane 4	1.63	-1.80
Plane 5	1.33	0.44
Plane 6	1.17	0.73
Plane 7	1.17	0.79
Plane 8	1.30	0.63
Plane 9	1.86	-1.31
Plane 10	3.69	-1.76
Plane 11	7.94	-2.67
Plane 12	23.70	-4.60

The Xenon effect is important for the peripheral planes, as they are exposed to low powers. The discrepancy increases from about 1% in the middle of the reactor to 24% at the extremity. The interpolation method provides about the same density in each bundle, which corresponds to the balance density at 615 kW. So, it tends to over-evaluate the Xenon effect at the boundary of the reactor.

The correction of Xenon densities improves the results. The discrepancies are under 1% in the middle of the core, and do not exceed 7% at the extremity.

The first plane of the reactor is representative of the distributed Xenon effects. While the concentrations are inaccurate with an interpolation, it is far better with the correction. The phenomenon is striking in the peripheral planes. As noticed beforehand, it does not seem to improve the power or the effective multiplication factor evaluation. As the errors on the computation of the Xenon occur locally, it does not affect the global behavior of the reactor.

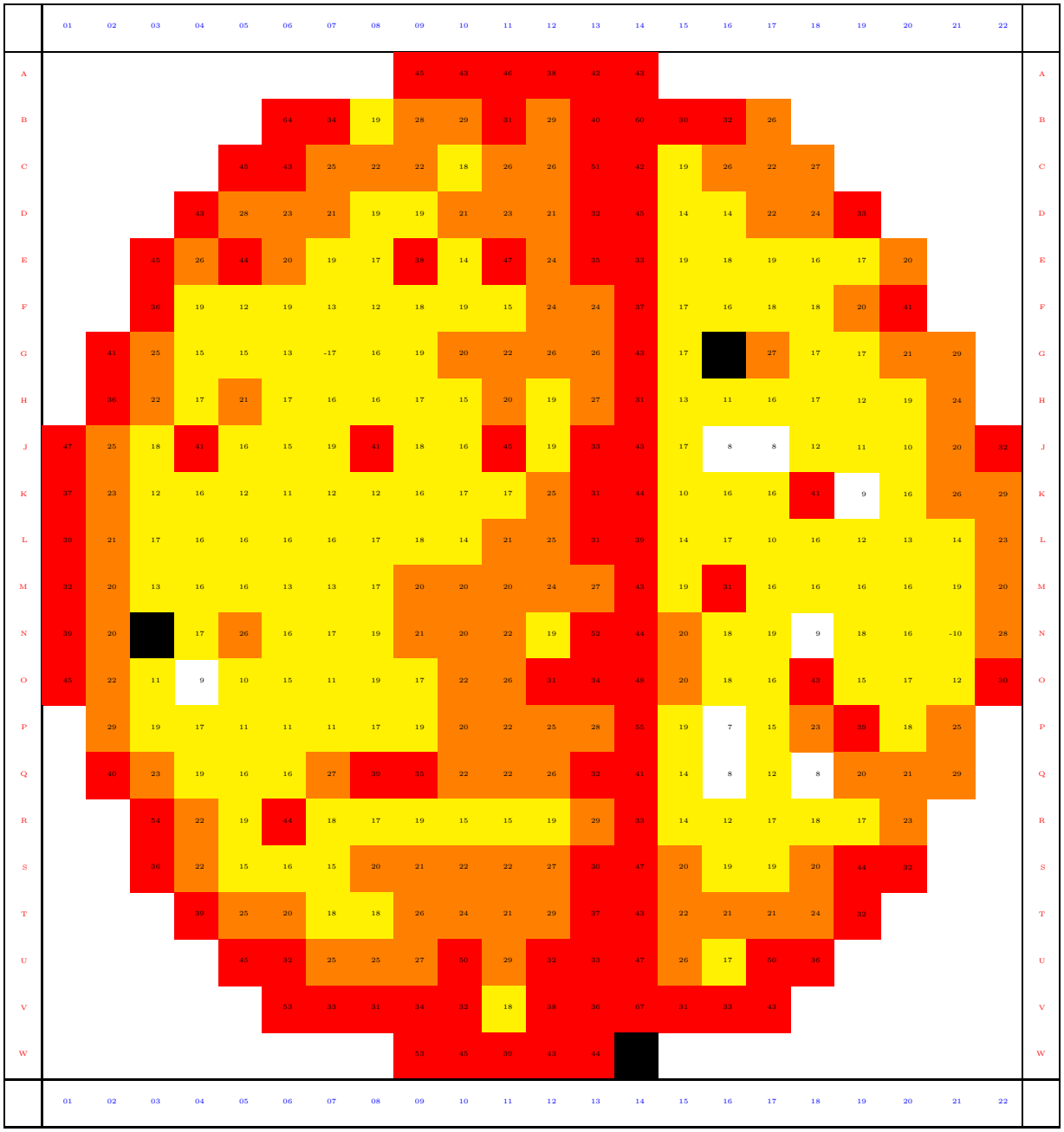

Figure 4.11 Relative differences ϵ_1^{plane} of Xenon-135 densities for the first plane at 3256.2 FPD (in %)

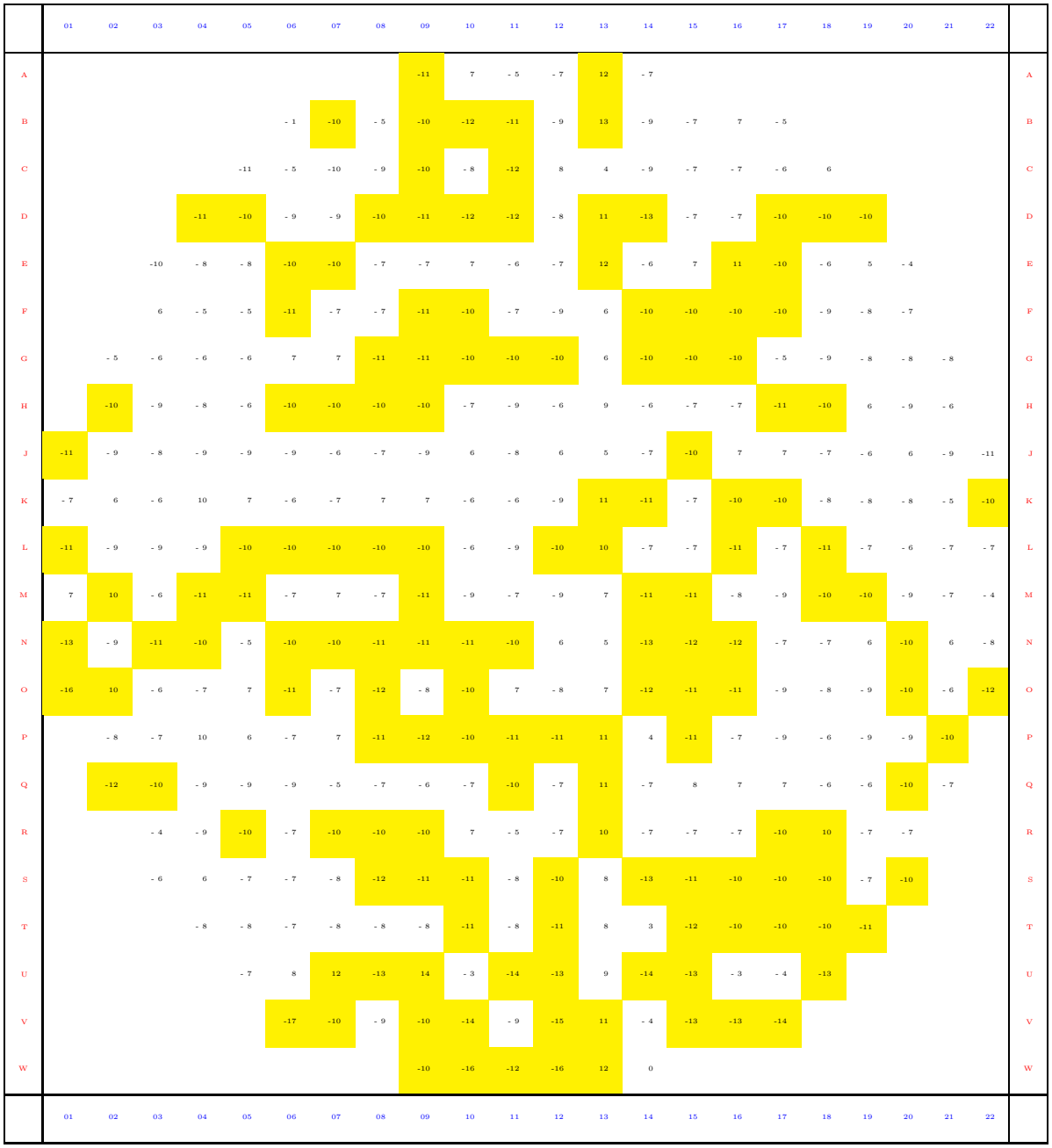

Figure 4.12 Relative differences ϵ_2^{plane} of Xenon-135 densities for the first plane at 3256.2 FPD (in %)

4.4 Conclusions

Four calculations of the CANDU-6 follow-up have been performed. The distributed Xenon effects are present when the evaluation of the densities is done by an interpolation calculation. Particularly, it occurs for the bundles located at the border of the reactor. The use of a Xenon-135 correction decreases considerably the errors. However, the impact on the multiplication factor is reduced because many bundles are operating at nominal powers. So, these bundles do not require a correction. The gain provided by the `XENON:` module is under 1 mk.

The micro-depletion shows a difference of 1 or 2 mk to the interpolation method, according to the type of homogenization. It does not change much the global behavior of the reactor. However, certain fission product concentrations are better evaluated using microscopic depletion. Their apparition is computed according to the local level of power instead of the bundle burnup. This is more realistic.

A micro-depletion calculation requires about twice as much more computational time as a macro-depletion calculation. Table 4.5 gives typical calculation time for a single CANDU-6 follow-up input file according to the two methods. The total calculation time is provided here for information but is highly dependent on the computer ressources. The interpolation step is present in both calculations and requires about the same time for each case. It is interesting to notice that the depletion and the on-line refueling step are much more demanding in case of micro-depletion. This is not surprising if we consider the way the depletion step is performed on both cases. The on-line refueling step using microscopic cross sections is a step that has specially been developped for the need of this work. This procedure consists in moving old fuel cell properties within the library while fresh fuel cells are inserted. At the end of the step, macroscopic cross sections are recomputed over the fuel-map geometry.

In this work, the goal was to compare interpolation and micro-depletion calculations. Hence, we produced a library of microscopic cross sections in both cases, so we can compare isotopic compositions. Within the framework of day-by-day production calculations, flux distribution and detector fits are the only useful quantities. The interpolation step time can thus be greatly reduced in macroscopic depletion.

Table 4.5 Elements of comparison of calculation time

Method	Macroscopic depletion	Microscopic depletion
Total calculation time	$\approx$ 7200 s	$\approx$ 14000 s
Interpolation step	$\approx$ 50%	$\approx$ 25%
Depletion step	$\approx$ 0%	$\approx$ 10%
On-line refueling	$\approx$ 0%	$\approx$ 40%

CONCLUSION

In this project, different studies had been carried out to test and validate the micro-depletion method in the chain of codes DRAGON/DONJON. The aim was to show the capability of the code DONJON to perform such calculations, and to compare with the classic method which is already implemented in the code. First, two different Benchmarks on CANDU-6 fuel assemblies had been studied. Then a full-core calculation was achieved to evaluate the impact of this method.

In macro-depletion, macroscopic cross sections were interpolated from the reactor database and used to compute the fuel depletion. In micro-depletion, isotopic densities were computed by the depletion solver `EVO:`. The reactor database previously generated in the lattice step was used to recover residual properties. Generally, this corresponds to properties coming from low-density and/or low-cross section nuclei. Other isotopes were extracted to be computed by `EVO:`. The microscopic cross sections used in micro-depletion are homogenized microscopic cross sections. As these quantities are burnup dependent, they had to be interpolated in a micro-depletion calculation.

Simple assemblies of fuel cells were studied. Our intent was to show the improvement provided by the micro-depletion method. Also, it provided a basis to be able to analyze the results coming from a full CANDU-6-core calculation. The main feature in comparison to a classic interpolation calculation was the computation of fission products densities. Low power depletion showed that interpolated properties could be inaccurate for certain isotopes. One of the most important fission products, Xenon-135, had to be recomputed by a new module. This solution brought an important gain in the results. However, Xenon-135 was not the only responsible for the error of reactivity calculation. A discrepancy remained in comparison to the DRAGON reference. The micro-depletion turned out to be more accurate than interpolation for low power depletion. Both methods are consistent for nominal power depletion.

The micro-depletion method was tested to deplete a CANDU-6 core. A fifty day depletion had been performed, with on-line refueling and adjusting the quantity of Boron. The generation of homogenized cross sections per fuel rings using DRAGON was made. It aimed to test the influence of depleting different rows of fuel pins within one CANDU-6 fuel bundle. The results showed that the gain was not worthwhile, since the additional computational

time was very large. In terms of k_{eff}, the micro-depletion turned out to be very close to the interpolation calculation. Even if the Xenon distribution calculation was inaccurate because of local power effects, it did not seem to have a large impact on the k_{eff}. Actually, the total power used to simulate the reactor was fixed to about 2000 MW. So, if the local power dropped at one location, it should increase elsewhere in the core. For instance, the powers of peripheral bundles were underestimated with the interpolation module and the powers at the middle of the core were overestimated.

This project gave the opportunity to show the capability of DONJON to carry out micro-depletion calculations. The emphasis was put on CANDU reactors. For this type of reactors, Xenon-135 or Samarium-149 are two important isotopes for the computation of reactivity. In other types of reactors, such as PWR or fast reactors, different types of fuels are used in different configurations. The use of a micro-depletion method to compute fission products or actinides concentrations can be tested in these reactors to see its influence in comparison to classic calculations.

REFERENCES

[1] A. Hébert, "Towards Version 4," in *Physor-2006 Workshop*, 2006.

[2] A. Pautz, H.-W. Bolloni, K.-A. Breith, R. van Geemert, J. Heinecke, G. Hobson, S. Merk, B. Pothet, and F. Curca-Tivig, "The ARTHEMIS core simulator: A central component in AREVA NPs code convergence project," in *M and C + SNA*, 2007.

[3] F. Hoareau, F. Laugier, and D. Couyras, "Elements of Validation of Microscopic depletion for the future EDF Calculation Scheme Based on APOLLO2 and COCAGNE Codes," in *Proceedings of ICAAP '08*, 2008.

[4] A. Hébert, *Applied Reactor Physics*. Presses Internationales Polytechnique, 2009.

[5] T. Reysset, "Development and qualification of advanced computational schemes for pressurized water reactors and creation of specific interfaces towards GRS full-core tools," Master's thesis, École Polytechnique de Montréal, 2009.

[6] J. Leppänen, "Development of a new monte-carlo reactor physics code," Ph.D. dissertation, Helsinki University of Technology, 2007.

[7] R. Sanchez, "Assembly homogenization techniques for core calculations," in *Progress in Nuclear Energy*, 2009.

[8] M. Dahmani, W. Shen, and B. Phelps, "Fuel-Pin Flux Reconstruction for CANDU Applications," in *CNS 2010*, 2010.

[9] G. Marleau, A. Hébert, and R. Roy, "A user guide for Dragon Version4," Institut de Génie Nucléaire, Tech. Rep. IGE-294, 2010.

[10] D. Sekki, A. Hébert, and R. Chambon, "A user guide for Donjon Version4," Institut de Génie Nucléaire, Tech. Rep. IGE-300, 2010.

[11] A. Hébert and R. Roy, "The Ganlib Version5 developer's guide," Institut de Génie Nucléaire, Tech. Rep. IGE-313, 2010.

[12] A. Hébert, "A user guide for Trivac Version4," Institut de Génie Nucléaire, Tech. Rep. IGE-293, 2010.

[13] R. Chambon, "A user guide for Optex Version 4.0," Institut de Génie Nucléaire, Tech. Rep. IGE-314, 2009.

[14] A. Hébert, G. Marleau, and R. Roy, "A description of the Dragon and Trivac Version4 data structures," Institut de Génie Nucléaire, Tech. Rep. IGE-295, 2010.

[15] D. Rozon, *Introduction à la cinétique des réacteurs nucléaires*. Éditions de l'École Polytechnique de Montréal, 1992.

[16] E. Varin, "Adjuster bank test simulation using the chain of codes Dragon/Donjon," Institut de Génie Nucléaire, Tech. Rep. IGE-228, 1999.

[17] E. Varin, A. Hébert, R. Roy, and J. Koclas, "A user guide for Donjon Version3.01," Institut de Génie Nucléaire, Tech. Rep. IGE-208, 2005.

[18] E. Varin, R. Roy, R. Baril, and G. Hotte, "CANDU-6 operation post-simulations using the reactor physics codes DRAGON/DONJON," in *Annals of Nuclear Energy*, 2004.

[19] E. Varin and G. Marleau, "CANDU reactor core simulations using fully coupled DRAGON and DONJON calculations," in *Annals of Nuclear Energy*, 2005.

APPENDIX A

Calculation schemes

In this appendix, an input file for a DONJON micro-depletion calculation is presented. This corresponds to the file used to generate results for the Benchmark 2, in Chapter 3.

A.1 Input file for an assembly calculation

```
*
*----------------------------------------------------------------------
*
*Purpose:
* Perform a micro-depletion calculation over a 6 by 6 assembly of
* CANDU-6 fuel cells using DONJON4
*
*Copyright:
* Copyright (C) 2011 Ecole Polytechnique de Montreal
* This library is free software; you can redistribute it and/or
* modify it under the terms of the GNU Lesser General Public
* License as published by the Free Software Foundation; either
* version 2.1 of the License, or (at your option) any later version.
*
*Author(s): M. Guyot
*
*----------------------------------------------------------------------
*
LINKED_LIST GEOM GEOM2 MATEX TRACK FMAP GEOEVO TRACKEVO GEOEVO2 MATEX2
            MICROLIB MICRO MACRO MACROLIB SYSTEM FLUX BURNUP CPO CPO2
            POWER NEWFLUX MACRO3 ;
MODULE GEO: USPLIT: TRIVAT: RESINI: NCR: TRIVAA: FLUD:
       EVO: DELETE: GREP: MACINI: FLPOW: END: TINST: ;
REAL
  Power  Delt Timec Timei Timef :=
  10.0   1.0   1.0   0.0   0.0 ;
```

```
REAL Keff ;
REAL PTOT := 4.96 ; ! power used for the interpolation
*---
* Set the 3D Geometry
*---
GEOM := GEO: :: CAR3D 6 6 1
   X- REFL X+ REFL
   MESHX 0.0 28.575 57.15 85.725 114.30 142.875 171.45
    SPLITX 1 1 1 1 1 1
   Y- REFL Y+ REFL
   MESHY 0.0 28.575 57.15 85.725 114.30 142.875 171.45
    SPLITY 1 1 1 1 1 1
   Z- REFL Z+ REFL MESHZ 0.0 49.53 SPLITZ 1
   MIX 1 1 1 1 1 1
       1 1 1 1 1 1
       1 1 1 1 1 1
       1 1 1 1 1 1
       1 1 1 1 1 1
       1 1 1 1 1 1 ;
GEOM2 MATEX := USPLIT: GEOM :: NGRP 2 MAXR 100
               NFUEL 1 FMIX 1  ;
TRACK := TRIVAT: GEOM2 :: MAXR 100 MCFD 1 ;

*---
* Set the fuel-map and the burnup of the fuel cells
*---
FMAP MATEX := RESINI: MATEX ::
  NCHAN 36 NBUND 1
  ::: GEO: CAR3D 6 6 1
           EDIT 0
   X- REFL X+ VOID MESHX 0.0 28.575 57.15 85.725 114.30 142.875 171.45
    SPLITX 1 1 1 1 1 1
   Y- REFL Y+ VOID MESHY 0.0 28.575 57.15 85.725 114.30 142.875 171.45
    SPLITY 1 1 1 1 1 1
   Z- REFL Z+ REFL MESHZ 0.0 49.53 SPLITZ 1
   MIX 1 1 1 1 1 1
```

```
       1 1 1 1 1 1
       1 1 1 1 1 1
       1 1 1 1 1 1
       1 1 1 1 1 1
       1 1 1 1 1 1  ;
   BUND-SIZE 28.575 28.575 49.53
   NXNAME "01" "02" "03" "04" "05" "06"
   NYNAME "A" "B" "C" "D" "E" "F"
   NCOMB ALL
   FUEL WEIGHT 19.85 ;
FMAP := RESINI: FMAP ::
  EDIT 1
  BTYPE INST-BURN
  INST-BVAL CHAN
    0. 0. 0. 0. 0. 0.
    0. 0. 0. 0. 0. 0.
    0. 0. 0. 0. 0. 0.
    0. 0. 0. 0. 0. 0.
    0. 0. 0. 0. 8000. 8000.
    0. 0. 0. 0. 8000. 8000. ;


*---
* Recover the fuel-map geometry used for micro-depletion
*---
GEOEVO := FMAP :: STEP UP "GEOMAP" ;
GEOEVO2 MATEX2 := USPLIT: GEOEVO :: NGRP 2 MAXR 100
               NFUEL 1 FMIX 1  ;
TRACKEVO := TRIVAT: GEOEVO2 :: MAXR 100 MCFD 1 ;

*---
* Recover the cell properties and first flux calculation
*---
SEQ_ASCII MULTICOMPO MULTICOMPO2 ;
CPO := MULTICOMPO ;
CPO2 := MULTICOMPO2 ;
```

```
MICRO := NCR: CPO2 :: EDIT 0
           NMIX 2
           COMPO CPO2 'moderator'
           MIX 2 FROM 1
           SET 'BURN' 0.
           MICRO ALL
           ENDMIX ;
MICROLIB := NCR: CPO FMAP :: EDIT 0
          TABLE CPO 'fuel' BURN
          MIX 1
          INST-BURN
          MICRO ALL
          ENDMIX ;
MACRO := MICRO :: STEP UP "MACROLIB" ;
MACROLIB := MICROLIB :: STEP UP "MACROLIB" ;

*----
* Flux calculation and initialization of the BURNUP
*----
MACRO3 MATEX := MACINI: MATEX MACRO MACROLIB :: EDIT 1 ;
SYSTEM := TRIVAA: MACRO3 TRACK :: EDIT 0 ;
FLUX := FLUD: SYSTEM TRACK ::  EDIT 0 EXTE 300 1.E-6 ;

POWER NEWFLUX := FLPOW: FMAP FLUX TRACK MATEX ::
            EDIT 1 PTOT <<PTOT>> BUND ;
BURNUP MICROLIB := EVO: MICROLIB NEWFLUX TRACKEVO ::
   SAVE 0.0 DAY POWR <<Power>> ;

GREP: FLUX :: GETVAL "K-EFFECTIVE" 1 >>Keff<< ;
ECHO "K-EFFECTIVE" Keff ;

*----
* Perform micro-depletion
*----
WHILE Timei Timec < DO
```

```
  EVALUATE Timef := Timei Delt + ;
* MICRO-DEPLETION
 BURNUP MICROLIB := EVO: BURNUP MICROLIB NEWFLUX TRACKEVO ::
  EDIT 3 DEPL <<Timei>> <<Timef>> DAY POWR <<Power>> ;
* INTERPOLATION FOR THE RESIDUAL ISOTOPE
FMAP := TINST: FMAP POWER :: TIME <<Delt>> DAY ;
MICROLIB := NCR: MICROLIB CPO FMAP :: EDIT 0
          RES
          TABLE CPO 'fuel' BURN
          MIX 1
          INST-BURN
          MICRO ALL
          ENDMIX ;

MACROLIB SYSTEM FLUX MACRO3 POWER NEWFLUX := DELETE:
MACROLIB SYSTEM FLUX MACRO3 POWER NEWFLUX ;
* FLUX CALCULATION
MACROLIB := MICROLIB :: STEP UP "MACROLIB" ;
MACRO3 MATEX := MACINI: MATEX MACRO MACROLIB :: EDIT 1 ;
SYSTEM := TRIVAA: MACRO3 TRACK :: EDIT 0 ;
FLUX := FLUD: SYSTEM TRACK ::  EDIT 0 EXTE 300 1.E-6 ADI 5 ;
* POWER CALCULATION
POWER NEWFLUX := FLPOW: FMAP FLUX TRACK MATEX ::
            EDIT 0 PTOT <<PTOT>>  BUND ;
BURNUP MICROLIB := EVO: BURNUP MICROLIB NEWFLUX TRACKEVO ::
   EDIT 3 SAVE <<Timef>> DAY POWR <<Power>> ;

GREP: FLUX :: GETVAL "K-EFFECTIVE" 1 >>Keff<< ;
ECHO "K-EFFECTIVE" Keff ;
*----
*  Change delta t for burnup and final time if required
*----
  IF Timef Timec = THEN
    IF Timec 10.0 = THEN
      EVALUATE Delt Timec := 10.0 150.0 ;
    ENDIF ;
```

```
    IF Timec 5.0 = THEN
      EVALUATE Delt Timec := 5.0 10.0 ;
    ENDIF ;
    IF Timec 1.0 = THEN
      EVALUATE Delt Timec := 4.0 5.0 ;
    ENDIF ;
  ENDIF ;
  EVALUATE Timei := Timef ;
ENDWHILE ;

END: ;
QUIT .
```

APPENDIX B

Follow-up

B.1 Main input file

A follow-up is composed of several calculation points. The chain is executed through a shell program. All the input files share a common part. An example of input file is given below at 3200.8 FPD.

The content of the CLE-2000 procedures called by the main file is not displayed. A brief description of each of them is given below :

SetModel	defines the geometry.
SetReflPro	specifies the reflector properties.
SetDevPro	specifies the devices properties.
SetPPM	specifies the poison load and the moderator purity.
SetFuelMap	defines the fuel map.
SetBurnup	specifies the initial burnups and powers of each bundle.
SetDevice	specifies the positions and the mixtures of each device.
SetDetect	specifies the detectors properties.
SetRefuel	creates a library containing the fresh fuel cell properties.

B.1.1 CLE-2000 procedures

SetModel

```
GEOM MATEX := SetModel :: <<MaxR>> ;
```

This CLE-2000 procedure is used to create two DONJON data structures. The input CLE-2000 variable corresponds to the maximum number of regions in the reactor geometry. Within the procedure, the fine mesh geometry of a CANDU-6 reactor is specified. The MATEX data structure is used to store information related to the reactor extended material index and geometry.

SetReflPro

```
MICRO := SetReflPro CPOREFL ;
```

This CLE-2000 procedure is used to create a library of microscopic cross sections for the reflector. The input file is a database generated at lattice level containing reflector properties.

SetDevPro

```
MACRO := SetDevPro MACRO GT ADJ ZCR STRUC ;
```

This CLE-2000 procedure is used to add the device materials to the library of macroscopic cross sections containing reflector materials. Four different databases are inputed.

SetPPM

```
MICRO := SetPPM MICRO :: <<INTRP>> <<ppm>> <<purmod>>  ;
```

This CLE-2000 procedure is used to set the Boron load and the moderator purity in the library of microscopic cross sections. The input CLE-2000 variables correspond respectively to the type of input library (either fuel-map library or library for the reflector properties), the Boron load (in ppm) and the moderator purity.

SetFuelMap

```
FMAP MATEX := SetFuelMap MATEX ;
```

This CLE-2000 procedure is used for modeling of the reactor fuel lattice. For example, the bidirectional refueling scheme is set. Reactor channels and bundles are identified by their specific name which correspond to the vertical and horizontal position in the fuel lattice.

SetBurnup

```
FMAP := SetBurnup FMAP ;
```

This CLE-2000 procedure is used to specify the burnups and the powers over the fuel-map geometry corresponding to the initial conditions for the CANDU-6 core follow.

SetDevice

```
DEVICE MATEX := SetDevice MATEX ;
```

This CLE-2000 procedure is used to create a DEVICE data structure and to modify the MATEX data structures. The DEVICE data structure is used to store several information related to the reactor devices. Records are created to store mixture indices, 3D-Cartesian

co-ordinates and insertion levels of rod-type or lzc-type devices. The rod-devices material mixtures are appended to the previous material index and the rod-devices indices are also modified, accordingly.

SetDetect

```
DETECT := SetDetect ;
```

This CLE-2000 procedure is used to create a DETECT data structure. This data structure contains detector positions and responses.

SetRefuel

```
MICNFUEL := SetRefuel CPOFUEL ;
```

This CLE-2000 procedure is used to create a LIBRARY data structure containing the fresh fuel cell properties. This library can thus be used for refueling during a micro-depletion core follow.

B.1.2 Interpolation method

```
************************************************************
* Input file :  JEPP_3200.8.x2m                            *
************************************************************

PROCEDURE SetModel SetReflPro SetDevPro SetPPM
          SetFuelMap SetBurnup SetDevice SetDetect ;

LINKED_LIST GEOM MATEX TRACK DEVICE MACRO FMAP NEWFLUX
             MACRO2 MACRO3 SYSTEM FLUX POWER
             DETECT MICRO MICROLIB MACROLIB ;

MODULE DSET: NCR: MACINI: TRIVAT: TRIVAA: NEWMAC: DETECT:
       FLUD: FLPOW: TINST: DELETE: GREP: END:   ;

REAL Keff ;
INTEGER MaxR := 30000 ;
REAL purmod ppm ;
  EVALUATE  purmod :=  99.96199799  ;
```

```
  EVALUATE  ppm :=  .206 ;
STRING INTRP := "REFL" ;
*--
* Set geometry
*--
GEOM MATEX := SetModel :: <<MaxR>> ;
TRACK := TRIVAT: GEOM :: MAXR <<MaxR>> MCFD 1 ;

*--
* Set device properties
*--
DEVICE MATEX := SetDevice MATEX ;
DEVICE := DSET: DEVICE ::
  EDIT 0
  LZC 1  LEVEL .5203 TIME 60. END
  LZC 2  LEVEL .4321 TIME 36. END
  LZC 3  LEVEL .4194 TIME 36. END
  LZC 4  LEVEL .3570 TIME 36. END
  LZC 5  LEVEL .4041 TIME 36. END
  LZC 6  LEVEL .3787 TIME 60. END
  LZC 7  LEVEL .2919 TIME 36. END
  LZC 8  LEVEL .4657 TIME 60. END
  LZC 9  LEVEL .4307 TIME 36. END
  LZC 10 LEVEL .6151 TIME 36. END
  LZC 11 LEVEL .4598 TIME 36. END
  LZC 12 LEVEL .3885 TIME 36. END
  LZC 13 LEVEL .4341 TIME 60. END
  LZC 14 LEVEL .4489 TIME 36. END
 ;

*--
* Set Detectors properties
*--
DETECT := SetDetect ;

*--
```

```
* Set fuel-map and burnups
*--
FMAP MATEX := SetFuelMap MATEX ;
SEQ_ASCII FUELMAP POW ;
FMAP := DELETE: FMAP ;
FMAP := FUELMAP ;
POWER := POW ;

*--
* Set a refuelling scheme
*--
FMAP := TINST: FMAP POWER  :: EDIT 0
  TIME 1.6  DAY REFUEL     CHAN H09  8
  TIME  .1  DAY REFUEL     CHAN V17  8
  TIME  .3  DAY      ;
POWER := DELETE: POWER ;

*--
* Recover the reflector properties from the database
*--
LINKED_LIST CPOREFL ;
SEQ_ASCII MULTICOMPO2 ;
CPOREFL := MULTICOMPO2 ;
MICRO := SetReflPro CPOREFL ;

*--
* Set the properties of the reflector : ppm and purity
*--
MICRO := SetPPM MICRO :: <<INTRP>> <<ppm>> <<purmod>>  ;
MACRO := MICRO :: STEP UP "MACROLIB" ;

*--
* Recover the device properties from the database
*--
LINKED_LIST GT ADJ ZCR STRUC ;
SEQ_ASCII GTUBEB RODB ZCPOB MATSTRB ;
```

```
GT := GTUBEB  ;
STRUC := MATSTRB ;
ZCR := ZCPOB   ;
ADJ := RODB   ;
MACRO := SetDevPro MACRO GT ADJ ZCR STRUC ;

*--
* Recover the fuel properties from the database
*--
LINKED_LIST CPOFUEL ;
SEQ_ASCII MULTICOMPO ;
CPOFUEL := MULTICOMPO ;
MICROLIB := NCR: CPOFUEL FMAP :: EDIT 0
          TABLE CPOFUEL 'fuel' BURN
          MIX 1 FROM 1
          INST-BURN
          MICRO ALL
          ENDMIX  ;
EVALUATE INTRP := "FUEL" ;
MICROLIB := SetPPM MICROLIB :: <<INTRP>> <<ppm>> <<purmod>>  ;
MACROLIB := MICROLIB :: STEP UP "MACROLIB" ;

*--
* Flux calculation and detectors readings
*--
MACRO2 MATEX := MACINI: MATEX MACRO MACROLIB :: EDIT 0 ;
MACRO3 MATEX := NEWMAC: MATEX MACRO2 DEVICE :: EDIT 0 ;
SYSTEM := TRIVAA: MACRO3 TRACK :: EDIT 0 ;
FLUX := FLUD: SYSTEM TRACK ::  EDIT 0 EXTE 100 1.E-6 ;
POWER NEWFLUX := FLPOW: FMAP FLUX TRACK MATEX ::
          EDIT 2 PTOT 2061.4 ;
DETECT := DETECT: DETECT NEWFLUX TRACK GEOM ::
       EDIT 5 REF 0 TIME 0.25 SIMEX ;

*--
* Destroy files
```

```
*--
SYSTEM MATEX TRACK MACRO MACROLIB DETECT GEOM := DELETE:
SYSTEM MATEX TRACK MACRO MACROLIB DETECT GEOM ;

GREP: FLUX :: GETVAL "K-EFFECTIVE" 1 >>Keff<< ;
ECHO "K-EFFECTIVE" Keff ;

*--
* Export files
*--
SEQ_ASCII FUELMAP2 POWER2 ;
FUELMAP2 := FMAP ;
POWER2 := POWER ;
END: ;
```

B.1.3 Micro-depletion method

```
************************************************************
* Input file :  JEPP_3200.8.x2m                            *
************************************************************

PROCEDURE SetModel SetReflPro SetDevPro SetPPM SetRefuel
          SetFuelMap SetBurnup SetDevice SetDetect ;

LINKED_LIST GEOM MATEX TRACK DEVICE MACRO FMAP NEWFLUX
            MACRO2 MACRO3 SYSTEM FLUX POWER MICNFUEL
            DETECT MICRO MICROLIB MACROLIB GEOEVO BURNUP
            TRACKEVO TRACKING MICROLIB2 CPOREFL CPOFUEL
            GEOEVO2 MATEX2 ;

MODULE DSET: NCR: MACINI: TRIVAT: TRIVAA: NEWMAC: DETECT:
       FLUD: FLPOW: TINST: DELETE: GREP: EVO: END: USPLIT:   ;

REAL Keff ;
INTEGER MaxR := 30000 ;
REAL purmod ppm ;
  EVALUATE  purmod :=  99.96199799  ;
  EVALUATE  ppm :=  .206 ;
STRING INTRP := "REFL" ;
REAL Power := 22.7739 ;

SEQ_ASCII MULTICOMPO MULTICOMPO2 ;
CPOREFL := MULTICOMPO2 ;
CPOFUEL := MULTICOMPO ;

*--
* Set geometry
*--
GEOM MATEX := SetModel :: <<MaxR>> ;
TRACK := TRIVAT: GEOM :: MAXR <<MaxR>> MCFD 1 ;
*--
* Create new fuel mixtures for refueling
```

```
*--
MICNFUEL := SetRefuel CPOFUEL ;

*--
* Set device properties
*--
DEVICE MATEX := SetDevice MATEX ;
DEVICE := DSET: DEVICE ::
  EDIT 0
  LZC 1  LEVEL .5203 TIME 60. END
  LZC 2  LEVEL .4321 TIME 36. END
  LZC 3  LEVEL .4194 TIME 36. END
  LZC 4  LEVEL .3570 TIME 36. END
  LZC 5  LEVEL .4041 TIME 36. END
  LZC 6  LEVEL .3787 TIME 60. END
  LZC 7  LEVEL .2919 TIME 36. END
  LZC 8  LEVEL .4657 TIME 60. END
  LZC 9  LEVEL .4307 TIME 36. END
  LZC 10 LEVEL .6151 TIME 36. END
  LZC 11 LEVEL .4598 TIME 36. END
  LZC 12 LEVEL .3885 TIME 36. END
  LZC 13 LEVEL .4341 TIME 60. END
  LZC 14 LEVEL .4489 TIME 36. END ;

*--
* Set Detectors properties
*--
DETECT := SetDetect ;

*--
* Set fuel-map and burnups
*--
FMAP MATEX := SetFuelMap MATEX ;
FMAP := DELETE: FMAP  ;
SEQ_ASCII POW FUELMAP;
POWER := POW ;
```

```
FMAP := FUELMAP ;

GEOEVO := FMAP :: STEP UP 'GEOMAP' ;
GEOEVO2 MATEX2 := USPLIT: GEOEVO :: NGRP 2 MAXR <<MaxR>>
               NFUEL 1  FMIX 1  ;
TRACKING := TRIVAT: GEOEVO2 :: MAXR <<MaxR>> MCFD 1 ;

*--
* Set a refuelling scheme for the residual
*--
FMAP := TINST: FMAP POWER :: EDIT 0
  TIME 1.6  DAY REFUEL     CHAN H09  8
  TIME  .1  DAY REFUEL     CHAN V17  8
  TIME  .3  DAY ;
POWER := DELETE: POWER ;

*--
* Recover the reflector properties from the database
*--
MICRO := SetReflPro CPOREFL ;

*--
* Set the properties of the reflector : ppm and purity
*--
MICRO := SetPPM MICRO :: <<INTRP>> <<ppm>> <<purmod>>  ;
MACRO := MICRO :: STEP UP "MACROLIB" ;

*--
* Recover the device properties from the database
*--
LINKED_LIST GT ADJ ZCR STRUC ;
SEQ_ASCII GTUBEB RODB ZCPOB MATSTRB ;
GT := GTUBEB  ;
STRUC := MATSTRB ;
ZCR := ZCPOB   ;
ADJ := RODB   ;
```

```
MACRO := SetDevPro MACRO GT ADJ ZCR STRUC ;

*--
* Importation of fuel properties and setting of the purity and poison load
*--
SEQ_ASCII LIB ;
MICROLIB := LIB ;
EVALUATE INTRP := "FUEL" ;
MICROLIB := SetPPM MICROLIB :: <<INTRP>> <<ppm>> <<purmod>>  ;

*--
* Refueling and interpolation of the residual
*--
MICROLIB2 FMAP := TINST: FMAP MICROLIB MICNFUEL :: EDIT 3
     REFUEL MICRO   CHAN H09  8
     REFUEL MICRO   CHAN V17  8 ;
MICROLIB := DELETE: MICROLIB ;
MICROLIB := MICROLIB2 ;
MICROLIB2 := DELETE: MICROLIB2 ;
MICROLIB := NCR: MICROLIB CPOFUEL FMAP :: EDIT 0
          RES
          TABLE CPOFUEL 'fuel' BURN
          MIX 1 FROM 1
          INST-BURN
          MICRO ALL
          ENDMIX  ;
MACROLIB := MICROLIB :: STEP UP "MACROLIB" ;

*--
* Flux and power calculation
*--
MACRO2 MATEX := MACINI: MATEX MACRO MACROLIB :: EDIT 0 ;
MACRO3 MATEX := NEWMAC: MATEX MACRO2 DEVICE :: EDIT 0 ;
SYSTEM := TRIVAA: MACRO3 TRACK :: EDIT 0 ;
FLUX := FLUD: SYSTEM TRACK ::  EDIT 0 EXTE 100 1.E-6 ;
```

```
GREP: FLUX :: GETVAL "K-EFFECTIVE" 1 >>Keff<< ;
ECHO "K-EFFECTIVE" Keff ;

POWER NEWFLUX := FLPOW: FMAP FLUX TRACK MATEX ::
          EDIT 2 PTOT 2061.4 BUND ;
*--
* Micro-depletion calculation
*--
BURNUP MICROLIB := EVO: MICROLIB NEWFLUX TRACKING ::
   SAVE 0.0 DAY POWR <<Power>> ;
BURNUP MICROLIB := EVO: BURNUP MICROLIB NEWFLUX TRACKING ::
  EDIT 0 DEPL 0.0 2.3 DAY POWR <<Power>> ;
*--
* Second flux and power calculation for detectors readings
*--
MACROLIB MACRO2 MACRO3 SYSTEM FLUX NEWFLUX POWER := DELETE:
MACROLIB MACRO2 MACRO3 SYSTEM FLUX NEWFLUX POWER ;
MACROLIB := MICROLIB :: STEP UP "MACROLIB" ;
MACRO2 MATEX := MACINI: MATEX MACRO MACROLIB :: EDIT 0 ;
MACRO3 MATEX := NEWMAC: MATEX MACRO2 DEVICE :: EDIT 0 ;
SYSTEM := TRIVAA: MACRO3 TRACK :: EDIT 0 ;
FLUX := FLUD: SYSTEM TRACK ::  EDIT 0 EXTE 100 1.E-6 ;

*---
* Compute the detectors reading after depletion
*---
POWER NEWFLUX := FLPOW: FMAP FLUX TRACK MATEX ::
            EDIT 0 PTOT 2061.4 ;
DETECT := DETECT: DETECT NEWFLUX TRACK GEOM ::
       EDIT 5 REF 0 TIME 0.25 SIMEX ;

GREP: FLUX :: GETVAL "K-EFFECTIVE" 1 >>Keff<< ;
ECHO "K-EFFECTIVE" Keff ;

*--
* Destroy files
```

```
*--
SYSTEM MATEX TRACK MACRO MACROLIB DETECT GEOM := DELETE:
SYSTEM MATEX TRACK MACRO MACROLIB DETECT GEOM ;

GREP: FLUX :: GETVAL "K-EFFECTIVE" 1 >>Keff<< ;
ECHO "K-EFFECTIVE" Keff ;

*--
* Export files
*--
SEQ_ASCII LIB2 FUELMAP2 POW2;
LIB2 := MICROLIB ;
FUELMAP2 := FMAP ;
POW2 := POWER ;

END: ;
```

B.2 Execution script file

B.2.1 Interpolation method

```
#!/bin/sh
echo "G2 follow-up with DONJON4"
rm *.result
rm *~
rdonjon4 Main.x2m ../Procs ../CPOs ../lib
mv Main+FUELMAP2 FUELMAP
mv Main+POWER2 POW

list="d43*"
for param in $list
  do
    rdonjon4 $param ../Procs ../CPOs FUELMAP POW ../lib
    param2="‘ echo $param | cut -d. -f1‘"
    mv $param2+FUELMAP2 FUELMAP
    mv $param2+POWER2 POW
    EXECDATE=‘date +"%y/%m/%d %H:%M:%S"‘
    echo "End of execution of " $param " at :" $EXECDATE
done
```

B.2.2 Micro-depletion method

```
#!/bin/sh
echo "G2 follow-up with DONJON4 in micro-depletion"
rm *.result
rm *~
rdonjon4 Main.x2m ../Procs ../CPOs ../lib
mv Main+LIB2 LIB
mv Main+FUELMAP2 FUELMAP
mv Main+POW2 POW

list="d43*"
for param in $list
  do
    rdonjon4 $param ../Procs ../CPOs FUELMAP POW LIB ../lib
```

```
    param2="` echo $param | cut -d. -f1`"
    mv $param2+LIB2 LIB
    mv $param2+FUELMAP2 FUELMAP
    mv $param2+POW2 POW
    EXECDATE=`date +"%y/%m/%d %H:%M:%S"`
    echo "End of execution of " $param " at :" $EXECDATE
done
```